iScience

CellPress

Article

Adult Influence on Juvenile Phenotypes by Stage-Specific Pheromone Production

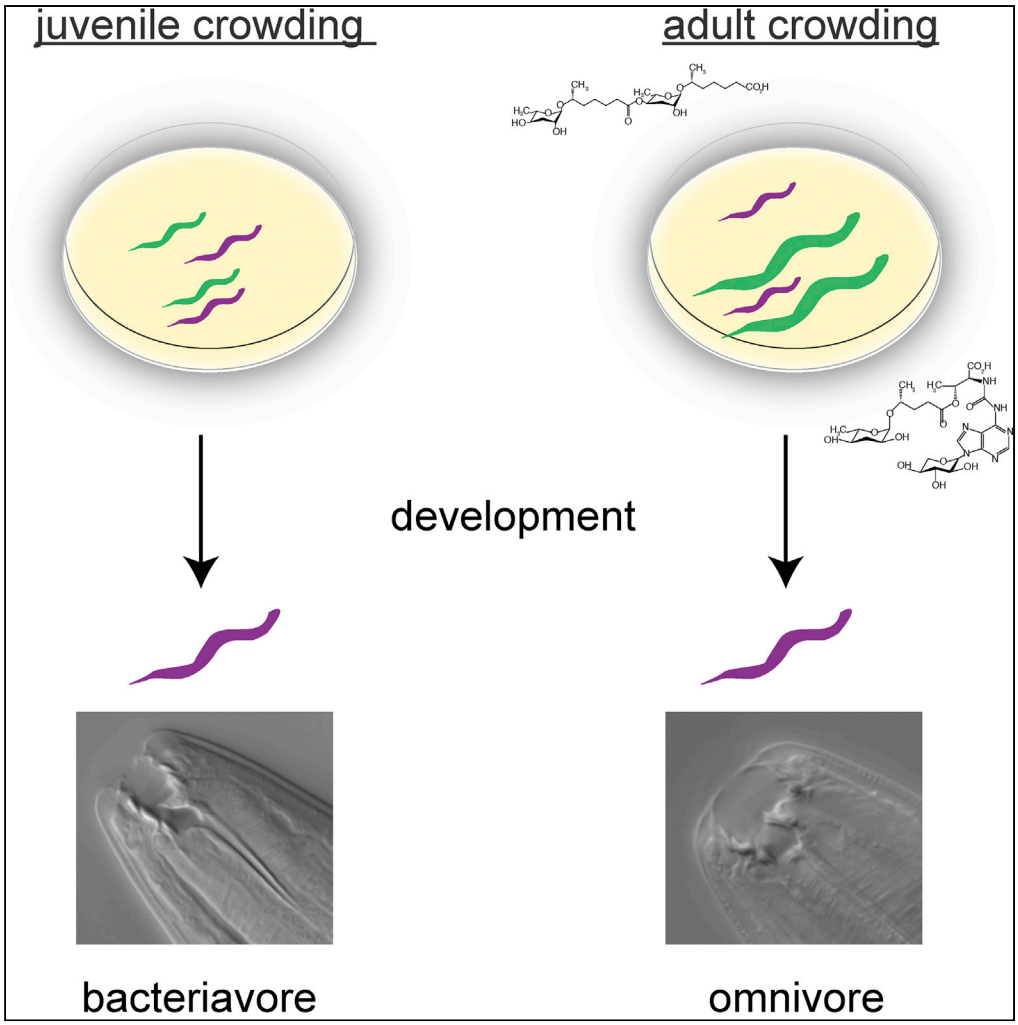

Michael S. Werner, Marc H. Claaßen, Tess Renahan, Mohannad Dardiry, Ralf J. Sommer

ralf.sommer@tuebingen.mpg.de

HIGHLIGHTS

Novel vital dye method for tracking mixed nematode populations

Adult, but not juvenile, crowding induces the omnivorous morph in *P. pacificus*

Omnivorous morph-inducing pheromones are produced late in development

Age class is an important component of density-dependent phenotypic plasticity

Werner et al., iScience *10*, 123–134
December 21, 2018
https://doi.org/10.1016/j.isci.2018.11.027

iScience

CellPress

Article

Adult Influence on Juvenile Phenotypes by Stage-Specific Pheromone Production

Michael S. Werner,[1,2] Marc H. Claaßen,[1,2] Tess Renahan,[1,2] Mohannad Dardiry,[1] and Ralf J. Sommer[1,3,*]

SUMMARY

Many animal and plant species respond to population density by phenotypic plasticity. To investigate if specific age classes and/or cross-generational signaling affect density-dependent plasticity, we developed a dye-based method to differentiate co-existing nematode populations. We applied this method to *Pristionchus pacificus*, which develops a predatory mouth form to exploit alternative resources and kill competitors in response to high population densities. Remarkably, adult, but not juvenile, crowding induces the predatory morph in other juveniles. High-performance liquid chromatography-mass spectrometry of secreted metabolites combined with genetic mutants traced this result to the production of stage-specific pheromones. In particular, the *P. pacificus*-specific di-ascaroside#1 that induces the predatory morph is induced in the last juvenile stage and young adults, even though mouth forms are no longer plastic in adults. Cross-generational signaling between adults and juveniles may serve as an indication of rapidly increasing population size, arguing that age classes are an important component of phenotypic plasticity.

INTRODUCTION

Population density is an important ecological parameter, with higher densities corresponding to increased competition for resources (Hastings, 2013). In addition to density-dependent selection (MacArthur, 1962; Travis et al., 2013), which operates on evolutionary timescales, some organisms can respond dynamically to population density through phenotypic plasticity. For example, plants can sense crowding by detecting the ratio of red (chlorophyll absorbing) to far red (non-absorbing) light, and respond by producing higher shoots (Dudley and Schmitt, 2015). Locusts undergo solitary to swarm (i.e., gregarious) transition as a result of increased physical contact (Pener and Simpson, 2009; Simpson et al., 2001). Intriguingly, population density can also have cross-generational effects, defined here as the density of one age group affecting the phenotypes of another. For example, adult crowding of the desert locust *Schistocerca gregaria* (Maeno and Tanaka, 2008; Simpson and Miller, 2007) and migratory locust *Locusta migratoria* (Chen et al., 2015; Ben Hamouda et al., 2011) also influences the egg size, number, and morphology of their progeny, high population densities of red squirrels elicit hormonal regulation in mothers to influence faster-developing offspring (Dantzer et al., 2013), and crowding in aphids can induce winged progeny from flightless parents (Slogget and Weisser, 2002, Sutherland, 1969). In many species, population density and cross-generational signaling are communicated by pheromones; however, the precise nature, mechanisms of induction, age specificity, and exact ecological role are not well understood.

Nematodes are a powerful model system to investigate the mechanisms of density-dependent plasticity because many small molecule pheromones that affect plastic phenotypes have been characterized (Butcher, 2017; Butcher et al., 2007; von Reuss et al., 2012). For example, in the model organism *Caenorhabditis elegans*, high population densities induce entry into a stress-resistant dormant "dauer" stage (Fielenbach and Antebi, 2008). The decision to enter dauer was revealed to be regulated by a family of small molecule nematode-derived modular metabolites (NDMMs) called ascarosides that act as pheromones (Butcher et al., 2007, 2008; Jeong et al., 2005). Ascarosides consist of an ascarylose sugar with a fatty acid side chain and modular head and terminal groups (Figure 1A). The level and composition of ascarosides were later shown to be dependent on sex (Chasnov et al., 2007; Izrayelit et al., 2012) and development (Kaplan et al., 2011), although it is thought that early larval development into dauer can be induced by pheromones from all developmental stages (Golden and Riddle, 1982). Subsequent studies revealed that specific NDMMs also regulate other life history traits, such as mating (Chasnov et al., 2007; Izrayelit et al., 2012), social behavior (Srinivasan et al., 2012), and developmental speed (Ludewig et al., 2017). Although NDMMs are broadly conserved (Choe et al., 2012; Dong et al., 2018; Markov et al., 2016), inter- and intraspecific competition have driven the evolution of distinct response regimes (different levels of sensitivity to the

[1]Department of Evolutionary Biology, Max Planck Institute for Developmental Biology, Tübingen 72076, Germany

[2]These authors contributed equally

[3]Lead Contact

*Correspondence: ralf.sommer@tuebingen.mpg.de

https://doi.org/10.1016/j.isci.2018.11.027

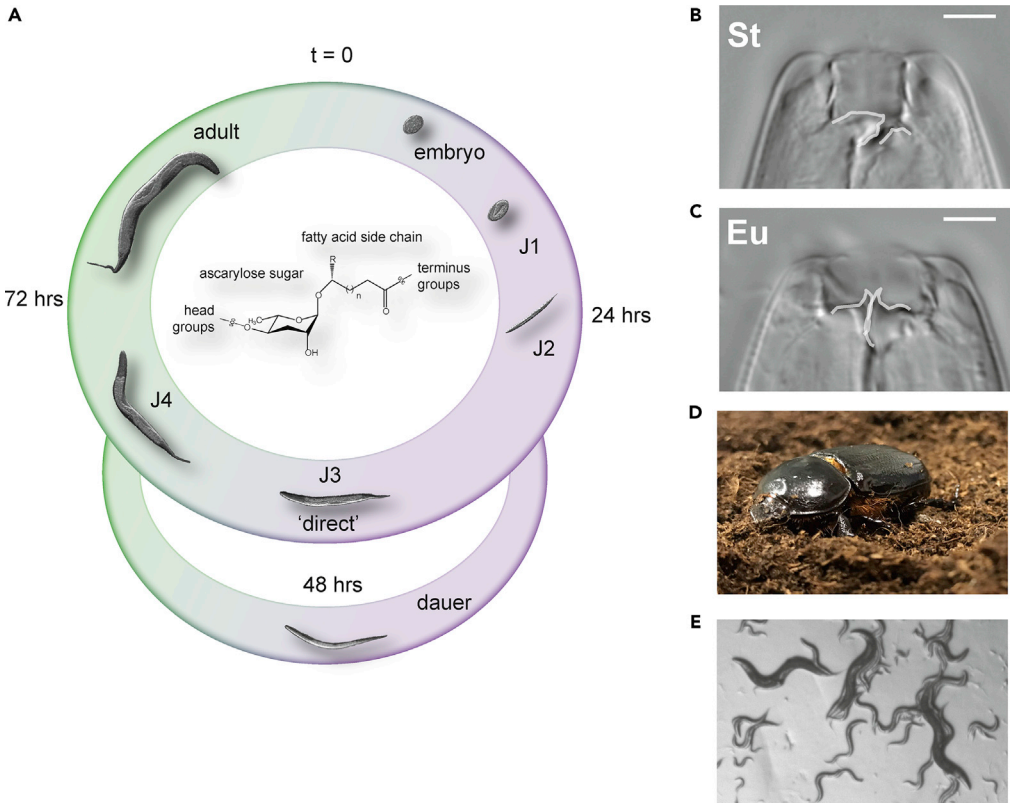

Figure 1. Life Cycle and Developmental Plasticity of the Model Nematode *Pristionchus pacificus*

(A) The life cycle of *P. pacificus* consists of four juvenile stages (J1–J4) until sexual maturation (adult hermaphrodites). Like many nematodes *P. pacificus* can enter a long-living "dormant" dauer state that is resistant to harsh environmental conditions. The decision to continue through the direct life cycle or enter dauer is regulated by small-molecule-excreted ascarosides (chemical structure adapted from Butcher, 2017).

(B and C) (B) *P. pacificus* can also adopt one of two possible feeding structures; either a microbivorous narrow mouth (stenostomatous, St) or (C) an omnivorous wide mouth (eurystomatous, Eu) with an extra tooth that can be utilized to kill and eat other nematodes or fungi. White lines indicate the presence of an extra tooth (right side) in the Eu morph or its absence in the St morph, and the dorsal tooth (left side), which is narrow and elongated (flint-like) in St and hook like in Eu. Scale bar, 5 μM.

(D) *P. pacificus* is often found in a necromenic association with beetles (e.g., shown here *Oryctes borbonicus*, photo taken by Tess Renahan) in the dauer state and resumes the free-living life cycle upon beetle death to feed on the ensuing microbial bloom.

(E) RSC017 mixed-staged worms on agar plates.

same pheromone, or sensitivity to different pheromones) for the same phenotypes (Bose et al., 2014; Choe et al., 2012; Diaz et al., 2014; Falcke et al., 2018; Greene et al., 2016). In addition, distinct plastic phenotypes have evolved that are regulated by more complex ascaroside structures (Bose et al., 2012).

In *Pristionchus pacificus*, a soil-associated nematode that is reliably found on scarab beetles (Figure 1A) (Herrmann et al., 2006, 2007; Sommer and McGaughran, 2013), an ascaroside dimer (dasc#1) that is not found in *C. elegans* regulates the development of a predatory mouth form (Bento et al., 2010; Bose et al., 2012; Sommer et al., 2017). Mouth-form plasticity represents an example of a morphological novelty that results in predatory behavior to exploit additional resources and kill competitors. Specifically, adult *P. pacificus* exhibit either a narrow stenostomatous (St) mouth (Figure 1B), which is restricted to bacterial feeding, or a wide eurystomatous (Eu) mouth with an extra denticle (Figure 1C), which allows for feeding on bacteria and fungi (Sanghvi et al., 2016), and predation on other nematodes (Wilecki et al., 2015). This type of phenotypic plasticity is distinct between direct, non-arrested development and indirect (dauer) development because the mouth form decision results in two alternative life history strategies in the adult (for review, see Sommer & Mayer, 2015). Recent studies in *P. pacificus* have begun to investigate the dynamics and succession of nematodes on decomposing beetle carcasses to better understand the ecological significance of mouth-form plasticity (Meyer et al., 2017). These studies revealed that on a carcass

(Figure 1D), *P. pacificus* exits the dauer diapause to feed on microbes, and then re-enters dauer after food sources have been exhausted, displaying a "boom-and-bust" ecology (Meyer et al., 2017; Sommer and McGaughran, 2013). Presumably different stages of this succession comprise different ratios of juveniles and adults, and recognizing the age structure of a population as a juvenile could provide predictive value for adulthood. However, it is unknown whether the mouth-form decision is sensitive to crowding by different age classes (example of crowding by different age groups, Figure 1E). More broadly, whereas age classes are known to be important for population growth and density-dependent selection (Hastings, 2013; Charlesworth, 1994; 1972), their role in phenotypic plasticity has thus far been largely unexplored.

Although nematodes have many experimental advantages, including easy laboratory culture and advanced genetic, genomic, and the aforementioned chemical tools, their small size has made investigations at the organismal level and in experimental ecology challenging. For example, no *in vivo* methodologies are currently available to label distinct populations without the need for transgenics, which is only available in select model organisms such as *C. elegans*, *P. pacificus*, and some of their relatives. Here, we combine a novel dye-staining method with the first developmental pheromone profiling in *P. pacificus* to study the potential effects of age on density-dependent plasticity. This vital dye method allows tracking adults with juveniles, or juveniles with juveniles, and can be applied to any nematode system that can be cultured under laboratory conditions. In contrast to dauer, we found that mouth form is strongly affected by cross-generational signaling. Specifically, only adult crowding induces the predatory morph, which is controlled by stage-specific pheromones.

RESULTS

A Vital Dye Method for Labeling Nematode Populations

To directly test if different age groups of *P. pacificus* influence mouth form, we required two synchronized populations to co-habit the same space, yet still be able to identify worms from different age groups. To do so, we developed a dye-staining methodology to robustly differentiate between nematode populations. After trying several vital dyes, we identified that neutral red (Thomas and Lana, 2008) and CellTracker Green BODIPY (Thermo) stain nematode intestines brightly and specifically to their respective channels (Figures 2A–2E and S1, Transparent Methods). These dyes stained all nematodes tested including *C. elegans* (Figure S2) and dauer larvae (Figures S3A and S3B). Both dyes lasted more than 3 days and neutral red >5 days (Figures S3C–S3G), allowing long-term tracking of mixed nematode populations. Importantly, neither neutral red nor CellTracker Green staining affected viability, developmental rate, or the formation of specific morphological structures, such as *P. pacificus* mouth form (Figure S4). Thus, neutral red and CellTracker Green allow specific labeling of worm populations to study age-dependent effects on phenotypes.

Adult but Not Juvenile Crowding Induces the Predatory Mouth Form in *P. pacificus*

To assess potential intra- or inter-generational influence on *P. pacificus* mouth form, we stained 200 juveniles stage 2 (J2s) of the highly St strain RSC017 (Figure 3A) with neutral red and added an increasing number of CellTracker Green-stained RSC017 adults or juveniles (J2s or J3/4s) (Figure 2F). After 3 days, we phenotyped red animals that had developed into adults. Almost half (48%) of the population developed an Eu mouth form with 500 adult animals, compared with less than 4% with 500 J2 or J3/4 juveniles ($n > 100$ from 2–5 independent biological replicates; for display, summed percentages are shown in Figures 3B–3D). We performed a direct statistical comparison between crowded plates and controls (no added crowding animals) for every number and stage of crowding. After multiple testing corrections, only 200 and 500 adult-crowded plates yielded significant differences compared with control (un-crowded) plates (*Bonferroni-corrected* $p = 6.9 \times 10^{-3}$ and $<2.2 \times 10^{-16}$, respectively, Fisher's exact test on Eu counts). To ascertain if there is a general difference between juvenile or adult crowding, we performed a binomial regression on replicate Eu count data, with stage (J2–J4 versus adults) and number of crowding animals included as fixed effects (Transparent Methods, Table S1). Indeed, we observed a significant difference between adult and juvenile crowding and the incidence of Eu morphs ($p = 1.32 \times 10^{-2}$).

We were also curious if dauers, which have a thickened cuticle and represent a distinct stage in the boom-and-bust life cycle of nematodes, could still respond to adults. Indeed, the same trend that was observed with juveniles was seen with dauers; only 200 and 500 adults significantly induced the Eu mouth form, albeit to a more muted extent (Figures 3E and 3F) (*Bonferroni-corrected* $p = 2.4 \times 10^{-2}$ and 7.3×10^{-5}, respectively; Fisher's exact test; and binomial regression between dauer and adult crowding $p = 2.96 \times 10^{-3}$).

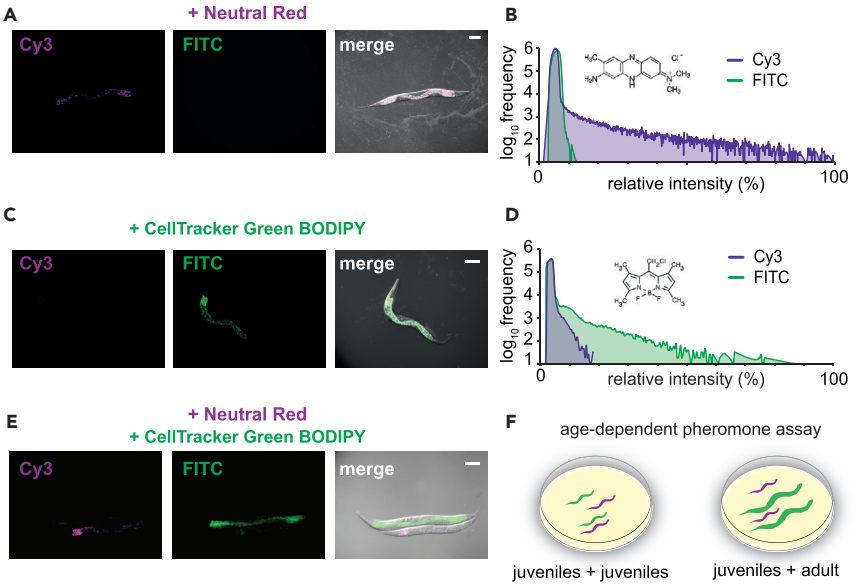

Figure 2. Vital Dye Method in Nematodes Allows Mixing Different Populations Together

(A) Neutral Red-stained adults (0.005% for 3 hours) imaged with Cy3 and FITC excitations and filters, and merged with DIC.

(B) An example of the relative intensities of fluorescence displayed as a histogram with the chemical structure of Neutral Red.

(C) CellTracker Green BODIPY (Thermo)-stained adults (50 μM for 3 hours) imaged with Cy3 and FITC excitations and filters, and merged with DIC.

(D) An example of the relative intensities of fluorescence displayed as a histogram with the chemical structure of CellTracker Green BODIPY.

(E) Combined worms from Neutral Red and CellTracker Green BODIPY staining on the same slide, merged with DIC.

(F) Age-dependent functional pheromone assay: experimental juveniles were stained with neutral red and challenged with CellTracker Green BODIPY-stained juveniles or adults on standard condition Nematode Growth Media (NGM) agar plates seeded with 300 μL OP50 *E. coli*. Three days later, only red-positive and green-negative adults were phenotyped.

With a total of 200 dauers and 500 adults, 25.7% of dauers became Eu, whereas only 1.8% of dauers become Eu on a plate containing 700 dauers (and no adults) (Figure 3F). Collectively, these data indicate that adult crowding specifically induces the Eu mouth form. However, it should be noted that because of the difficulty in obtaining a pure J4 culture from RSC017s, we cannot rule out that crowding by large numbers of J4s could also induce the Eu morph.

Even though we did not detect a mouth-form switch in large populations of J2s or dauers, and food was still visible on plates containing the most animals (500 "crowders"), we could not completely rule out the possible effect of food availability on mouth form. As a proxy for starvation, we conducted assays with greatly increased numbers of juveniles from 1,000 to 10,000 that would rapidly deplete bacterial food. We noticed a stark cliff in the fraction of animals that reach adulthood at 4,000–5,000 juveniles, arguing that food is a limiting resource at this population density (Figure 3G). Importantly, however, in these plates we still did not see a shift in mouth form (Figure 3H) ($p = 0.99$, binomial regression, Table S1). With an overwhelming 10,000 worms on a plate, 5.8% were Eu, compared with 48% in the presence of only 500 adults. Although longer-term starvation may have an impact on mouth form, under our experimental conditions it appears to be negligible.

Late-Stage Secretions Induce the Eu Mouth Form

As the mouth-form decision in *P. pacificus* can be influenced by NDMMs (Bose et al., 2012), we wondered if the difference in Eu induction between adults and juveniles resulted from differences in secreted pheromones. To test this hypothesis, we added secretions from 24- and 72-hr cultures of RSC017 and the laboratory strain RS2333 (which is highly Eu) to RSC017 juveniles. We found that the 72-hr (late juvenile stage

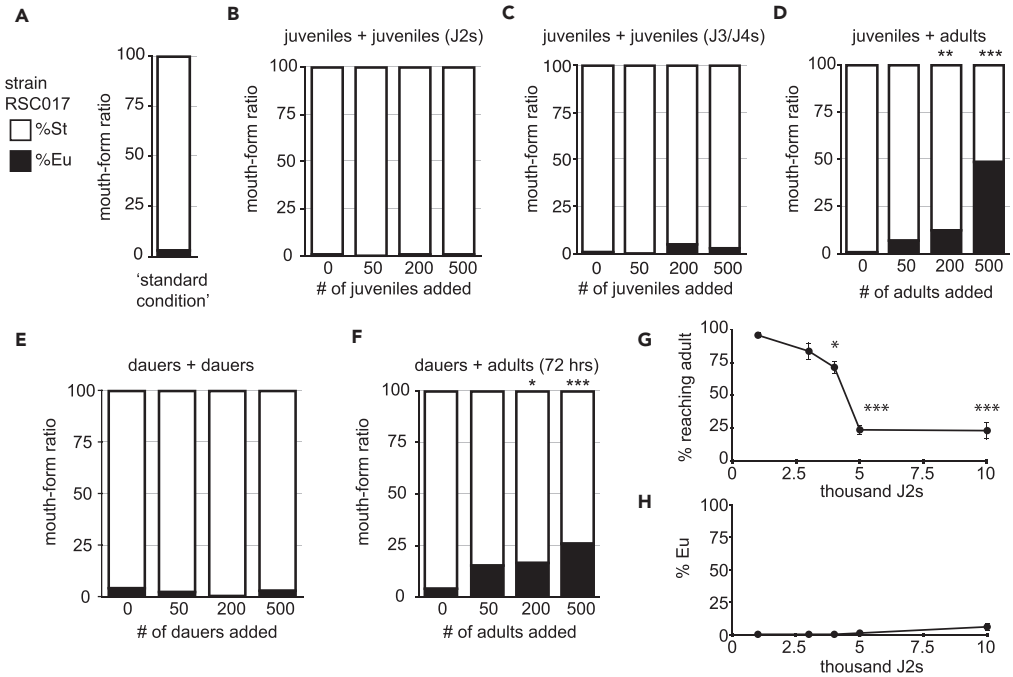

Figure 3. Vital Dye Method Demonstrates Adult-Specific Density Effect on Mouth Form

(A–F) (A) The wild isolate RSC017 grown in standard conditions (5 young adults passed to fresh plates, progeny phenotyped 4 days later) are highly stenostomatous (<10%, *n* = 102). Mouth form ratios of neutral red-stained J2s (B–D) and dauers (E and F), with increasing number of CellTracker Green-stained competitors (total number of animals *n* > 100 per experiment, with 3–5 independent biological replicates for J2 and adult crowding, and 2 for J3/J4s). Overall significance between strain and age was determined by a binomial linear regression (see Transparent Methods), and pairwise comparisons were assessed by Fisher's exact test on summed Eu counts (***p < 0.001, **p < 0.01, *p < 0.05). Mouth forms were phenotyped at 40–100× on a Zeiss Axio Imager 2 light microscope.

(G and H) (G) Percent reaching adulthood and percent Eu of those that reached adulthood (H) after increasing numbers of J2s were added to standard 6-cm Nematode Growth Media (NGM) agar plates with 300 μL OP50 *E. coli* bacteria (n = 2 biological replicates, with total *n* > 200 for percent reaching adulthood, and total n > 100 for mouth form. Significance was determined by a binomial regression; Error bars represent standard deviation of the two biological replicates).

4/adult, Figure S4H; Werner et al., 2017) secretions from both strains led to a significant increase in the Eu morph relative to the 24-hr (early juvenile J2) secretions ($p = 5.27 \times 10^{-6}$, 1.33×10^{-3}, respectively, Fisher's exact test on Eu counts relative to S-medium controls, n = 2-4 biological replicates; for display, summed percentages are shown in Figure 4). To confirm that the effect was caused by ascaroside pheromones, we exposed RSC017 juveniles to supernatant from a *P. pacificus daf-22.1;daf-22.2* double mutant, which exhibits virtually no ascaroside production in both *C. elegans* and *P. pacificus* (Golden and Riddle, 1985; Markov et al., 2016). Again, early juvenile secretion had no impact on Eu frequency, but in contrast to wild-type supernatants, we observed no significant increase in Eu frequency with the 72-hr secretions ($p = 0.8324$, Fisher's exact test, Figure 4). Thus, late-stage NDMMs induce development of the Eu mouth form.

Developmental-Staged NDMM Profiles Reveal Age-Specific Synthesis of dasc#1

Next, we investigated whether the different effects of early and late pheromones are ones of dosage, or of identity. To determine the potential age-specific differences in pheromones, we profiled *P. pacificus* NDMM levels in two strains and at three time points throughout development with high-performance liquid chromatography-mass spectrometry (Figures 5A, 5B, and S5). We performed a linear regression with the area under the curve of each NDMM chromatogram (Figure S5A) as the response variable. Stage and strain were modeled as fixed effects, and because we performed separate regression analyses for each pheromone, we adjusted the resulting p values for multiple testing using false discovery rate (FDR) (see Table S2 for p and FDR values between stage and strain). We observed that among developmental stages there were significant differences in the levels of ascr#9, ascr#12, npar#1, and dasc#1, and that dasc#1,

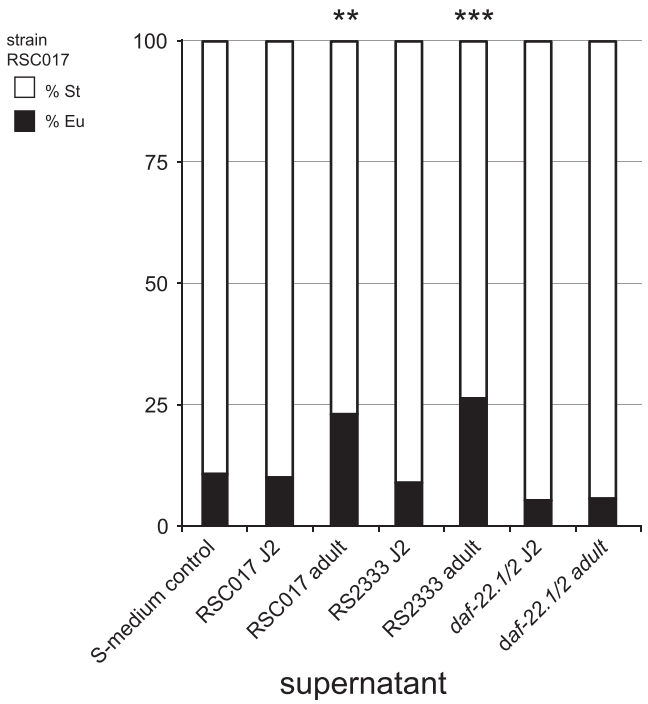

Figure 4. Late-Stage Secretions Induce Predatory Morph in Juveniles

Highly St strain RSC017 juveniles were exposed to 24- and 72-hr supernatants of its own strain, and to the 24- and 72-hr supernatants of the highly Eu strain RS2333. Mouth form was phenotyped 3 days later. Worms exposed to 24-hr secretions remained highly St, whereas worms exposed to 72-hr secretions had a small but significant increase in Eu morphs ($p < 0.05$, Fisher's exact test). Supernatants from the double mutant *daf-22.1/2*, which has deficient ascaroside pheromone production (Golden and Riddle, 1985; Markov et al., 2016), did not elicit increases in Eu from either 24- or 72-hr supernatants. Worms exposed to the S-media control also remained highly St. n = 4 independent biological replicates for RS2333 and *daf-22.1/2* secretions, and n = 2 independent biological replicates for RSC017 secretions, with an average count of 55 animals per replicate. For display, total Eu and St counts are presented as percentages (*** $p < 0.001$, **$p < 0.01$).

ubas#1, and ubas#2 are affected by both stage and strain (FDR<0.05). Interestingly, dasc#1 is the most potent known Eu-inducing pheromone when tested as a single synthesized compound, whereas npar#1 is both an Eu- and a dauer-inducing pheromone (Bose et al., 2012). Closer inspection revealed dasc#1, npar#1, and ascr#9 increase throughout development in both strains, and dasc#1 peaks at 72 hr in RS2333 (Figures 5C and 5D and 5F–5I, $p < 0.05$, Student's two-tailed t test between 72 and 24 hr for each NDMM in both strains, and 72 and 48 hr for dasc#1 in RS2333, Table S3). Intriguingly, the trajectory of dasc#1 appeared "binary/off-on" in both strains; in some replicates dasc#1 levels were undetectable, whereas others were high and virtually no replicates exhibited intermediate levels (Figures 5F and 5G). In fact, our statistical model for dasc#1 fits better if we assume cubic rather than linear growth (model difference Akaike information criterion, $\Delta AIC = 3.958$). In contrast, ascr#9, which was also statistically increased but does not affect known plastic phenotypes (Bose et al., 2012), displayed a more gradual increase in both strains (Figures 5E, 5J, and 5K), and the model fits better with linear growth ($AIC_{linear} - AIC_{cubic} = -1.208$). Meanwhile, the induction pattern of npar#1 appears particular to each strain, although our linear model did not detect significant strain effects. Thus the kinetics of induction appears to be NDMM specific, which may be related to their roles in phenotypic plasticity.

We were interested to know if there was a transcriptional signal that would correlate with the increase in NDMMs throughout development. An analysis of previously published RNA sequencing data (Baskaran et al., 2015) reveals an ~5-fold increase in transcription of the thiolase *Ppa-daf-22.1* (Figure S6A) between J2 and J4/adults, the most downstream enzyme in the β-oxidation pathway of ascaroside synthesis. However, this enzyme is responsible for the last step in synthesizing many NDMMs in addition to dasc#1, npar#1, and ascr#9, so other enzymes must also be involved, and identifying them is an area of active research.

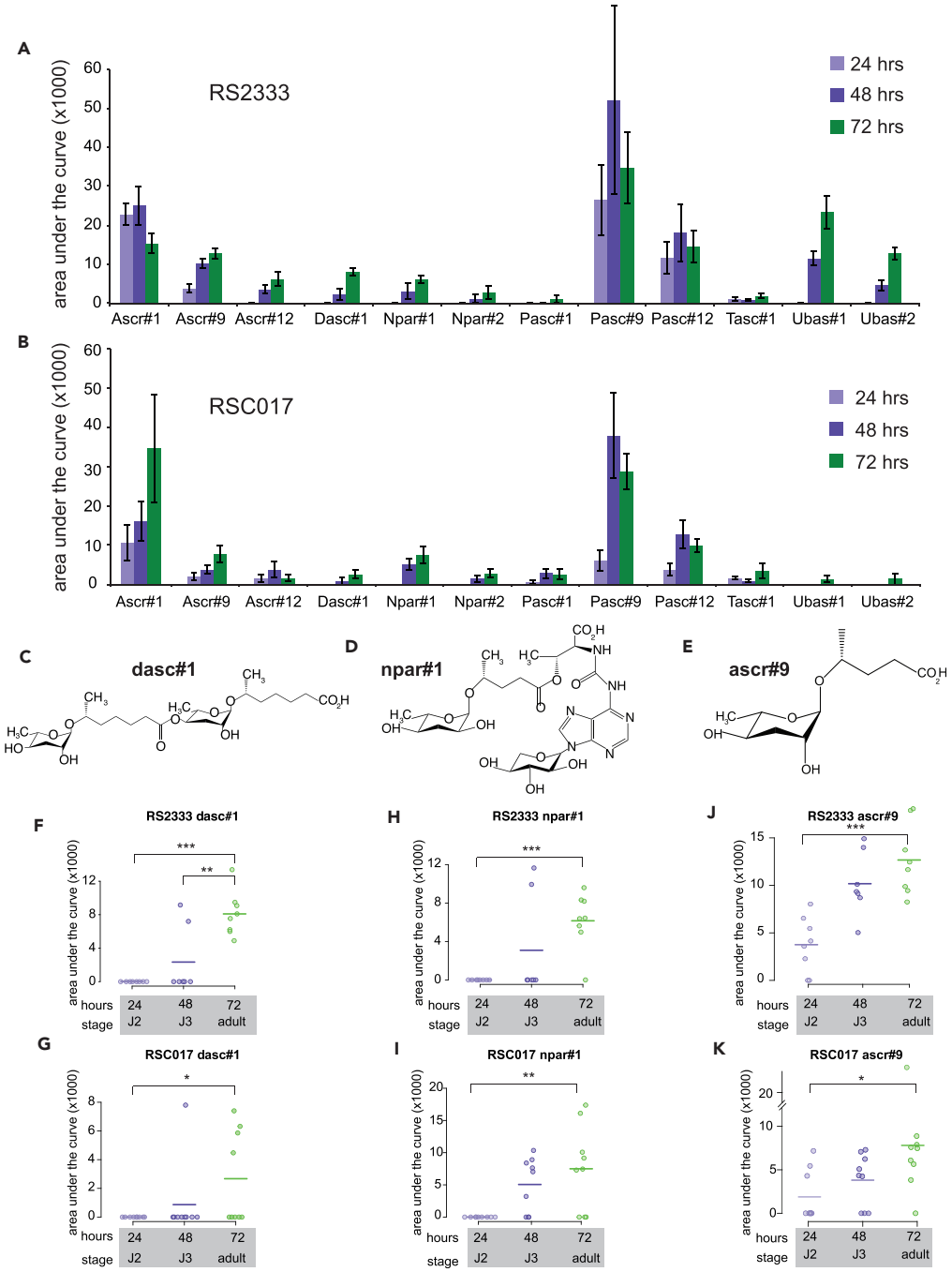

Figure 5. Time-Resolved Nematode-Derived Modular Metabolites (NDMMs) in *Pristionchus pacificus*

(A and B) (A) Time-resolved secretion profile of nematode-derived modular metabolites from the wild-type laboratory strain RS2333 and (B) wild isolate RSC017. In both strains, at 24 hr cultures represent predominantly J2 stage worms, at 48 hr a mix of J2–J4, and at 72 hr predominantly adults in RSC017 (90%, Figure S4H) and a mix of J4/adults in RS2333 (Werner et al., 2017). Data are presented as the mean of 8 (RS2333) and 9 (RSC017) biological replicates, and error bars represent the standard error of mean (SEM).

(C–E) Chemical structures of age-specific NDMMs (C) dasc#1, (D) npar#1, and (E) ascr#9, as described in the Small Molecule Identifier Database (http://www.smid-db.org/), produced in ChemDraw.

(F–K) Time-resolved abundance of (F and G) dasc#1, (H and I) npar#1, and (J and K) ascr#9 NDMMs in RS2333 and RSC017. Each data point represents a biological replicate, and for comparison with (A and B) lines represent mean abundance. p values calculated by a 2-tailed Student's t test (***$p < 0.001$, **$p < 0.01$, *$p < 0.05$).

In principle, the increase in abundance of dasc#1, npar#1, and ascr#9 throughout development could be a result of a concomitant increase in body mass. We used WormSizer (Moore et al., 2013) to measure the size of RSC017 animals from each time point and then normalized NDMM abundances by volume. We found a 1.1-fold difference in body volume between 24- and 48-hr samples, and a 1.3-fold difference between 24- and 72-hr samples. However, normalizing by these factors did not affect the significance of dasc#1, npar#1, or ascr#9 between time points (Tables S3 and S4; Figures S6B–S6D). We also suspect that size is not the only factor because no other compounds significantly increased throughout development in our linear model. Finally, we profiled the endo-metabolome of eggs and found appreciable amounts of ascr#1, #9, and #12 and pasc#9, but little to no traces of other ascaroside derivatives (Figure S5C), suggesting age-specific synthesis, rather than release from ascarosides already present in eggs/J1. Together, these results suggest that the observed increase in ascr#9, npar#1, and dasc#1 over time corresponds to age-specific production. The observation that dasc#1 is produced specifically during the juvenile-to-adult transition is especially intriguing because adults are no longer able to switch mouth forms, hinting at cross-generational signaling.

DISCUSSION

Here, we introduce a novel dye-based method that allowed us to assess cross-generational influence on mouth form. Our results demonstrate that adult crowding induces the Eu predatory morph, and that this effect is, at least partially, a result of age-specific pheromones. In doing so, we provide the first multi-stage time series of pheromone production in *P. pacificus*, which shows that dasc#1 exhibits a surprising switch-like induction pattern. Collectively, our results suggest that adults represent a "critical age group" with respect to phenotypic plasticity. The fact that adults also represent the critical age group with respect to population density (Charlesworth, 1972) may explain their outsized contribution to induction of the Eu morph. The presence of adults may indicate rapidly decreasing bacterial resources, and thus developing the Eu morph will allow worms to exploit additional resources and kill competitors.

Our developmental profiling revealed an increase in two NDMMs that affect plastic phenotypes. Given that J4s can produce dasc#1/npar#1, we believe the lack of effect of the J3/J4 stage compared with adults in our mixed-culture assay simply reflects the more consistently present and higher amounts of dasc#1/npar#1 produced at 72 hr and experienced for longer periods of time. The observation that this trend occurs regardless of body size implies that these molecules are programmed for stage-specific production. The "off-on" induction kinetics might reflect a population-level feedback loop, wherein the production of excess pheromones is based on a threshold level of previously produced pheromones. The variability observed at 48 hr for dasc#1/npar#1 might reflect biological variability in developmental timing and/or technical variation in staging. It is also worth noting that although npar#1 is the major dauer-inducing pheromone in *P. pacificus* (Bose et al., 2012), we did not observe dauer juveniles in any of our dye-crowding assays. Thus, it seems that mouth-form phenotype is the first-level plastic response to population density. Presumably higher concentrations are required for dauer induction, reflecting a calculated response strategy depending on the level of crowding or duration of starvation. Interestingly, the effect of 72-hr supernatants was noticeably less (23%–26% Eu) than the physical presence of adult worms (up to 48% with only 500 adults). It is difficult to compare pheromone concentrations between experiments, but presumably worms in the vital dye assay experienced a greater local concentration as they were in direct contact with each other for longer periods of time, and were also older than the 72-hr supernatant assayed in our pheromone profiling. However, it is also formally possible that other factors, like increased physical contact, can induce the Eu morph.

The maximum levels of Eu reached in our mixed culture experiment was ~50% with 500 adults, begging the question if this could be pushed further by using greater levels of crowding. However, this proved technically difficult due to food constraints with excess worms. Adding more food (OP50 LB) began to decrease the integrity of the agar, which made recovering animals for phenotyping difficult. Importantly, adults do not seem capable of eating other adults, which might otherwise push the Eu frequency even higher as a defense strategy. We also suspect that there are unknown trade-offs between the Eu and St mouth forms, which may manifest in a "ceiling" of the Eu frequency even under more crowded conditions.

Among the many environmental influences on mouth form (Werner et al., 2017), population density and starvation are perhaps the most ecologically relevant. However, teasing apart these two factors has

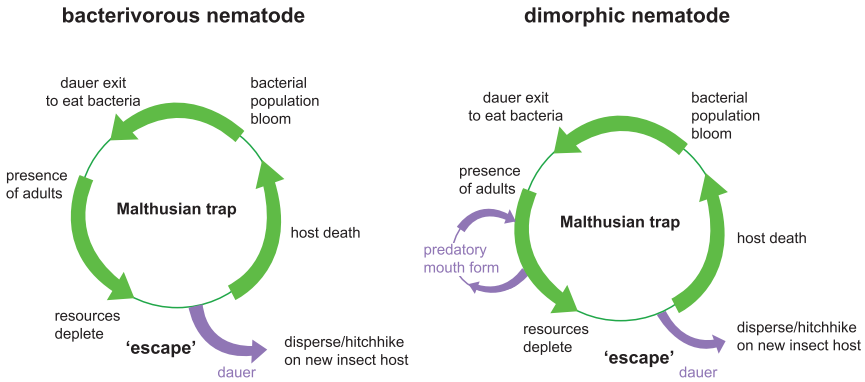

Figure 6. Conceptual Model of the Role of Critical Age Classes in Mouth-Form Phenotypic Plasticity

Conceptual life cycle models of monomorphic or dimorphic mouth-form nematodes. In an isolated niche such as a decaying insect carcass, at some point microbial food supplies will run out, leading to a Malthusian catastrophe. Nematodes escape this trap by entering the dauer state and dispersing, and re-starting the cycle. Dimorphic nematodes may sense the impending "catastrophe" earlier by recognizing an abundance of adults in the population, and switching to the Eu morph to exploit new resources and kill competitors. By analogy to economic models, the mouth-form switch is a technological innovation to temporarily escape a Malthusian resource trap.

been a challenge (Bento et al., 2010). Here, we demonstrate that whereas a strong shift is observed with age-specific pheromones, no such effect was seen under limited resource conditions. Thus, age-specific crowding is sufficient to induce the Eu mouth form. Nevertheless, this does not preclude that long-term starvation could also have an effect. Determining the relative contributions of these factors to mouth form will be important to better understand the sophisticated ecological response strategies of *P. pacificus*, nematodes, and phenotypic plasticity in general.

Why do adults and not juveniles affect mouth form? For now we can only speculate, but given that St animals develop slightly faster (Serobyan et al., 2013), there may be a "race" to sexual maturation in emergent populations at low densities. However, as the nematode population increases, there will likely be a commensurate decrease in bacterial populations. When faced with competition from other nematodes, *P. pacificus* has a particular advantage in developing the Eu morph; their expanded dietary range includes other nematode competitors. Indeed, when nematode prey is the only available food source, animals with the Eu morph have longer lifespans and more progeny than animals with the St morph (Serobyan et al., 2014). When resources become depleted as the population size increases, *C. elegans* and other monomorphic nematodes may enter dauer and disperse (Frézal and Félix, 2015). However, in St-biased dimorphic strains of *P. pacificus*, juveniles may switch to the Eu morph in response to adults as a first-level indication of rapidly increasing population size (Figure 6). Then, after prolonged starvation and crowding, worms will presumably enter dauer. By analogy to economic models of population growth (Malthus, 1826; Trewavas, 2002) mouth-form plasticity is a "technological innovation" to temporarily escape a Malthusian resource trap.

The evolution of dimorphic mouth forms is one among myriad nematode ecological strategies. For example, entomopathogenic nematodes release their symbiont bacteria in insect hosts to establish their preferred food source, and the bacteria can release antibiotics to kill off competing bacteria and fungi (Griffin, 2012). Some free-living species, like those of the genus *Oscheius*, may refrain from combat and stealthily feed and reproduce amid warring entomopathogenic species (Campos-Herrera, 2015a). Interspecific killing also occurs in gonochoristic species, in which both mated and virgin males are killed, implying fighting not just for mates but for resources as well (O'Callaghan et al., 2014; Zenner et al., 2014). Different reproductive strategies also exist, and hermaphroditic species have an advantage over gonochoristic species when colonizing a new niche, such as an insect carcass (Campos-Herrera, 2015b). Meanwhile, insect hosts and colonizing nematodes have their own distinct pheromone-based attraction and toxicity (Cinkornpumin et al., 2014; Renahan and Hong, 2017). Finally, the renaissance of *C. elegans* sampling from around the world (Cook et al., 2017; Evans et al., 2016; Félix et al., 2013; Petersen et al., 2014; Poullet and Braendle, 2015) is rapidly building a resource of wild isolates that will almost certainly have different and fascinating ecologies. We hope our method for labeling and then combining different

nematode populations on the same plate will aid in studies to identify these strategies. Perhaps the time is also ripe to complement these studies with more sophisticated ecological modeling that can lead to testable hypotheses.

Although beyond the scope of this manuscript, the cross-generational communication we observed could in principle reflect an intended signal from adults to juveniles, i.e., kin selection (Bourke, 2014). However, we favor a more simplistic view that juveniles have evolved to recognize late-stage metabolites. Regardless of these interpretations, our results argue that age classes are a critical factor in density-dependent plasticity, as has been theorized in density-dependent selection (Charlesworth, 1994).

Limitations of the Study

Given the ubiquity of certain traits in reproductive adults and their contribution to population growth, we suspect similar results will be found in other systems. However, it may depend on the phenotype and system being studied. For example, the population dynamics of this nematode (fast hermaphroditic reproduction) may be sufficiently different from other species such that our findings have limited generalizability. In addition, our method of staining different populations, although fast and easy, is particular to nematodes. Finally, to what extent our ecological interpretations exist in nature remains to be determined.

METHODS

All methods can be found in the accompanying Transparent Methods supplemental file.

SUPPLEMENTAL INFORMATION

Supplemental Information includes Transparent Methods, six figures, and four tables and can be found with this article online at https://doi.org/10.1016/j.isci.2018.11.027.

ACKNOWLEDGMENTS

We would like to thank all members of the Sommer lab, Dr. Talia Karasov, Dr. Hernan Burbano, and Moises Exposito-Alonso for guidance with statistical analysis, and Dr. Adrian Striet (Max Planck Institute) and Dr. Cameron Weadick (University of Sussex) for thoughtful critique and discussion. The work was funded by the Max Planck Society.

AUTHOR CONTRIBUTIONS

M.S.W. and R.J.S. conceived of the project. M.H.C. conducted pheromone profiling with help from M.S.W. and T.R. M.S.W. and T.R. designed and conducted dye-labeling experiments. T.R. and M.H.C. performed supernatant experiments. M.D. and M.S.W. considered ecological implications. M.S.W. and T.R. wrote the manuscript with input and edits from all authors.

DECLARATION OF INTERESTS

The authors declare no competing interests.

Received: August 15, 2018
Revised: November 15, 2018
Accepted: November 15, 2018
Published: December 21, 2018

REFERENCES

Baskaran, P., Rödelsperger, C., Prabh, N., Serobyan, V., Markov, G.V., Hirsekorn, A., and Dieterich, C. (2015). Ancient gene duplications have shaped developmental stage-specific expression in *Pristionchus pacificus*. BMC Evol. Biol. *15*, 185.

Ben Hamouda, A., Tenaka, S., Ben Hamouda, M.H., and Bouain, A. (2011). Density-dependent phenotypic plasticity in body coloration and morphometry and its transgenerational changes in the migratory locust, Locusta migratoria. J. Entomol. Nematol. *3*, 105–116.

Bento, G., Ogawa, A., and Sommer, R.J. (2010). Co-option of the hormone-signalling module dafachronic acid–DAF-12 in nematode evolution. Nature *466*, 494–497.

Bose, N., Meyer, J.M., Yim, J.J., Mayer, M.G., Markov, G.V., Ogawa, A., Schroeder, F.C., and Sommer, R.J. (2014). Natural variation in dauer pheromone production and sensing supports intraspecific competition in nematodes. Curr. Biol. *24*, 1536–1541.

Bose, N., Ogawa, A., von Reuss, S.H., Yim, J.J., Ragsdale, E.J., Sommer, R.J., and Schroeder, F.C. (2012). Complex small-molecule architectures regulate phenotypic plasticity in a nematode. Angew. Chem. Int. Ed. *51*, 12438–12443.

Bourke, A.F.G. (2014). Hamilton's rule and the causes of social evolution. Philos. Trans. R. Soc. Lond. B Biol. Sci. *369*, 20130362.

Butcher, R.A. (2017). Small-molecule pheromones and hormones controlling nematode development. Nat. Chem. Biol. *13*, 577–586.

Butcher, R.A., Fujita, M., Schroeder, F.C., and Clardy, J. (2007). Small-molecule pheromones that control dauer development in *Caenorhabditis elegans*. Nat. Chem. Biol. *3*, 420–422.

Butcher, R.A., Ragains, J.R., Kim, E., and Clardy, J. (2008). A potent dauer pheromone component in *Caenorhabditis elegans* that acts synergistically with other components. Proc. Natl. Acad. Sci. U S A *105*, 14288–14292.

Campos-Herrera, R. (2015a). Traditional and molecular detection methods reveal intense interguild competition and other multitrophic interactions associated with native entomopathogenic nematodes in Swiss tillage soils. Plant Soil *389*, 237–255.

Campos-Herrera, R. (2015b). Nematode Pathogenesis of Insects and Other Pests (Springer).

Charlesworth, B. (1994). Evolution in Age-Structured Populations (Cambridge Univ. Press).

Charlesworth, B. (1972). Selection in populations with overlapping generations. III. Conditions for genetic equilibrium. Theor. Popul. Biol. *3*, 377–395.

Chasnov, J.R., So, W.K., Chan, C.M., and Chow, K.L. (2007). The species, sex, and stage specificity of a *Caenorhabditis* sex pheromone. Proc. Natl. Acad. Sci. U S A *104*, 6730–6735.

Chen, B., Li, S., Ren, Q., Tong, X., Zhang, X., and Kang, L. (2015). Paternal epigenetic effects of population density on locust phase-related characteristics associated with heat-shock protein expression. Mol. Ecol. *24*, 851–862.

Choe, A., von Reuss, S.H., Kogan, D., Gasser, R.B., Platzer, E.G., Schroeder, F.C., and Sternberg, P.W. (2012). Ascaroside signaling is widely conserved among nematodes. Curr. Biol. *22*, 772–780.

Cinkornpumin, J.K., Wisidagama, D.R., Rapoport, V., Go, J.L., Dieterich, C., Wang, X., Sommer, R.J., and Hong, R.L. (2014). A host beetle pheromone regulates development and behavior in the nematode *Pristionchus pacificus*. Elife *3*, e03229.

Cook, D.E., Zdraljevic, S., Roberts, J.P., and Andersen, E.C. (2017). CeNDR, the *Caenorhabditis elegans* natural diversity resource. Nucleic Acids Res. *45*, D650–D657.

Dantzer, B., Newman, A.E.M., Boonstra, R., Palme, R., Boutin, S., Humphries, M.M., and McAdam, A.G. (2013). Density triggers maternal hormones that increase adaptive offspring growth in a wild mammal. Science *340*, 1215–1217.

Diaz, S.A., Brunet, V., Lloyd-Jones, G.C., Spinner, W., Wharam, B., and Viney, M. (2014). Diverse and potentially manipulative signalling with ascarosides in the model nematode *C. elegans*. BMC Evol. Biol. *14*, 46.

Dong, C., Reilly, D.K., Bergame, C., Dolke, F., Srinivasan, J., and von Reuss, S.H. (2018). Comparative ascaroside profiling of *Caenorhabditis* exometabolomes reveals species-specific (ω) and (ω – 2)-hydroxylation downstream of peroxisomal β-oxidation. J. Org. Chem. *83*, 7109–7120.

Dudley, S.A., and Schmitt, J. (2015). Testing the adaptive plasticity hypothesis: density-dependent selection on manipulated stem length in impatiens capensis. Am. Nat. *147*, 445–465.

Evans, K.S., Zhao, Y., Brady, S.C., Long, L., McGrath, P.T., and Andersen, E.C. (2016). Correlations of genotype with climate parameters suggest *Caenorhabditis elegans* niche adaptations. G3 (Bethesda) *7*, 289–298.

Falcke, J.M., Bose, N., Artyukhin, A.B., Rödelsperger, C., Markov, G.V., Yim, J.J., Grimm, D., Claassen, M.H., Panda, O., Baccile, J.A., et al. (2018). Linking genomic and metabolomic natural variation uncovers nematode pheromone biosynthesis. Cell Chem. Biol. *25*, 787–796.e12.

Félix, M.-A., Jovelin, R., Ferrari, C., Han, S., Cho, Y.R., Andersen, E.C., Cutter, A.D., and Braendle, C. (2013). Species richness, distribution and genetic diversity of *Caenorhabditis* nematodes in a remote tropical rainforest. BMC Evol. Biol. *13*, 10.

Fielenbach, N., and Antebi, A. (2008). *C. elegans* dauer formation and the molecular basis of plasticity. Genes Dev. *22*, 2149–2165.

Frézal, L., and Félix, M.-A. (2015). The natural history of model organisms: *C. elegans* outside the Petri dish. Elife *4*, e05849.

Golden, J.W., and Riddle, D.L. (1982). A pheromone influences larval development in the nematode *Caenorhabditis elegans*. Science *218*, 578–580.

Golden, J.W., and Riddle, D.L. (1985). A gene affecting production of the *Caenorhabditis elegans* dauer-inducing pheromone. Mol. Gen. Genet. *198*, 534–536.

Greene, J.S., Brown, M., Dobosiewicz, M., Ishida, I.G., Macosko, E.Z., Zhang, X., Butcher, R.A., Cline, D.J., McGrath, P.T., and Bargmann, C.I. (2016). Balancing selection shapes density-dependent foraging behaviour. Nature *539*, 254–258.

Griffin, C.T. (2012). Perspectives on the behavior of entomopathogenic nematodes from dispersal to reproduction: traits contributing to nematode fitness and biocontrol efficacy. J. Nematol. *44*, 177–184.

Hastings, A. (2013). Population Biology: Concepts and Models (Springer).

Herrmann, M., Mayer, W.E., and Sommer, R.J. (2006). Nematodes of the genus *Pristionchus* are closely associated with scarab beetles and the Colorado potato beetle in Western Europe. Zoology *109*, 96–108.

Herrmann, M., Mayer, W.E., Hong, R.L., Kienle, S., Minasaki, R., and Sommer, R.J. (2007). The nematode *Pristionchus pacificus* (Nematoda: Diplogastridae) is associated with the oriental beetle exomala orientalis (Coleoptera: Scarabaeidae) in Japan. Zoolog. Sci. *24*, 883–889.

Izrayelit, Y., Srinivasan, J., Campbell, S.L., Jo, Y., Reuss, von, S.H., Genoff, M.C., Sternberg, P.W., and Schroeder, F.C. (2012). Targeted metabolomics reveals a male pheromone and sex-specific ascaroside biosynthesis in *Caenorhabditis elegans*. ACS Chem. Biol. *7*, 1321–1325.

Jeong, P.-Y., Jung, M., Yim, Y.-H., Kim, H., Park, M., Hong, E., Lee, W., Kim, Y.H., Kim, K., and Paik, Y.-K. (2005). Chemical structure and biological activity of the *Caenorhabditis elegans* dauer-inducing pheromone. Nature *433*, 541–545.

Kaplan, F., Srinivasan, J., Mahanti, P., Ajredini, R., Durak, O., Nimalendran, R., Sternberg, P.W., Teal, P.E.A., Schroeder, F.C., Edison, A.S., et al. (2011). Ascaroside expression in *Caenorhabditis elegans* is strongly dependent on diet and developmental stage. PLoS One *6*, e17804.

Ludewig, A.H., Gimond, C., Judkins, J.C., Thornton, S., Pulido, D.C., Micikas, R.J., Döring, F., Antebi, A., Braendle, C., and Schroeder, F.C. (2017). Larval crowding accelerates *C. elegans* development and reduces lifespan. PLoS Genet. *13*, e1006717.

MacArthur, R.H. (1962). Some generalized theorems of natural selection. Proc. Natl. Acad. Sci. U S A *48*, 1893–1897.

Maeno, K., and Tanaka, S. (2008). Maternal effects on progeny size, number and body color in the desert locust, *Schistocerca gregaria*: density- and reproductive cycle-dependent variation. J. Insect Physiol. *54*, 1072–1080.

Malthus, T.R. (1826). An Essay on the Principle of Population (Cambridge University Press).

Markov, G.V., Meyer, J.M., Panda, O., Artyukhin, A.B., Claaßen, M., Witte, H., Schroeder, F.C., and Sommer, R.J. (2016). Functional conservation and divergence of daf-22 paralogs in *Pristionchus pacificus* Dauer development. Mol. Biol. Evol. *33*, 2506–2514.

Meyer, J.M., Baskaran, P., Quast, C., Susoy, V., Rödelsperger, C., Glöckner, F.O., and Sommer, R.J. (2017). Succession and dynamics of *Pristionchus* nematodes and their microbiome during decomposition of *Oryctes borbonicus* on La Réunion Island. Environ. Microbiol. *19*, 1476–1489.

Moore, B.T., Jordan, J.M., and Baugh, L.R. (2013). WormSizer: high-throughput analysis of nematode size and shape. PLoS One *8*, e57142.

O'Callaghan, K.M., Zenner, A.N.R.L., Hartley, C.J., and Griffin, C.T. (2014). Interference competition in entomopathogenic nematodes: male *Steinernema* kill members of their own and other species. Int. J. Parasitol. *44*, 1009–1017.

Pener, M.P., and Simpson, S.J. (2009). Locust phase polyphenism: an update. Adv. Insect Physiol. *36*, 196–201.

Petersen, C., Dirksen, P., Prahl, S., Strathmann, E.A., and Schulenburg, H. (2014). The prevalence of *Caenorhabditis elegans* across 1.5 years in

selected North German locations: the importance of substrate type, abiotic parameters, and *Caenorhabditis* competitors. BMC Ecol. *14*, 4.

Poullet, N., and Braendle, C. (2015). Sampling and isolation of *C. elegans* from the natural habitat. Methods Mol. Biol. *1327*, 221–229.

Renahan, T., and Hong, R.L. (2017). A species-specific nematocide that results in terminal embryogenesis. J. Exp. Biol. *220*, 3238–3247.

Sanghvi, G.V., Baskaran, P., Röseler, W., Sieriebriennikov, B., Rödelsperger, C., and Sommer, R.J. (2016). Life history responses and gene expression profiles of the nematode *Pristionchus pacificus* cultured on Cryptococcus yeasts. PLoS One *11*, e0164881.

Serobyan, V., Ragsdale, E.J., and Sommer, R.J. (2014). Adaptive value of a predatory mouth-form in a dimorphic nematode. Proc. R. Soc. Lond. B Biol. Sci. *281*, 20141334–20141989.

Serobyan, V., Ragsdale, E.J., Müller, M.R., and Sommer, R.J. (2013). Feeding plasticity in the nematode *Pristionchus pacificusis* influenced by sex and social context and is linked to developmental speed. Evol. Dev. *15*, 161–170.

Simpson, S.J., Despland, E., Hägele, B.F., and Dodgson, T. (2001). Gregarious behavior in desert locusts is evoked by touching their back legs. Proc. Natl. Acad. Sci. U S A *98*, 3895–3897.

Simpson, S.J., and Miller, G.A. (2007). Maternal effects on phase characteristics in the desert locust, *Schistocerca gregaria*: a review of current understanding. J. Insect Physiol. *53*, 869–876.

Sloggett, J.J., and Weisser, W.W. (2002). Parasitoids induce production of the dispersal morph of the pea aphid, *Acyrthosiphon pisum*. Oikos *98* (2), 323–333.

Sommer, R.J., and Mayer, M.G. (2015). Toward a synthesis of developmental biology with evolutionary theory and ecology. Annu. Rev. Cell Dev. Biol. *31*, 453–471.

Sommer, R.J., and McGaughran, A. (2013). The nematode *Pristionchus pacificus* as a model system for integrative studies in evolutionary biology. Mol. Ecol. *22*, 2380–2393.

Sommer, R.J., Dardiry, M., Lenuzzi, M., Namdeo, S., Renahan, T., Sieriebriennikov, B., and Werner, M.S. (2017). The genetics of phenotypic plasticity in nematode feeding structures. Open Biol. *7*, https://doi.org/10.1098/rsob.160332.

Srinivasan, J., von Reuss, S.H., Bose, N., Zaslaver, A., Mahanti, P., Ho, M.C., O'Doherty, O.G., Edison, A.S., Sternberg, P.W., and Schroeder, F.C. (2012). A modular library of small molecule signals regulates social behaviors in *Caenorhabditis elegans*. PLoS Biol. *10*, e1001237.

Sutherland, O.R.W. (1969). The role of crowding in the production of winged forms by two strains of the pea aphid, *Acyrthosiphon pisum*. J. Insect Physiol. *15*, 1385–1410.

Thomas, M.C., and Lana, P.D.C. (2008). Evaluation of vital stains for free-living marine nematodes. Braz. J. Oceanogr. *56*, 249–251.

Travis, J., Leips, J., and Rodd, F.H. (2013). Evolution in population parameters: density-dependent selection or density-dependent fitness? Am. Nat. *181*, S9–S20.

Trewavas, A. (2002). Malthus foiled again and again. Nature *418*, 668–670.

von Reuss, S.H., Bose, N., Srinivasan, J., Yim, J.J., Judkins, J.C., Sternberg, P.W., and Schroeder, F.C. (2012). Comparative metabolomics reveals biogenesis of ascarosides, a modular library of small-molecule signals in *C. elegans*. J. Am. Chem. Soc. *134*, 1817–1824.

Werner, M.S., Sieriebriennikov, B., Loschko, T., Namdeo, S., Lenuzzi, M., Dardiry, M., Renahan, T., Sharma, D.R., and Sommer, R.J. (2017). Environmental influence on *Pristionchus pacificus* mouth form through different culture methods. Sci. Rep. *7*, 7207.

Wilecki, M., Lightfoot, J.W., Susoy, V., and Sommer, R.J. (2015). Predatory feeding behaviour in *Pristionchus* nematodes is dependent on phenotypic plasticity and induced by serotonin. J. Exp. Biol. *218*, 1306–1313.

Zenner, A.N.R.L., O'Callaghan, K.M., and Griffin, C.T. (2014). Lethal fighting in nematodes is dependent on developmental pathway: male-male fighting in the entomopathogenic nematode *Steinernema longicaudum*. PLoS One *9*, e89385.

ISCI, Volume *10*

Supplemental Information

Adult Influence on Juvenile Phenotypes by Stage-Specific Pheromone Production

Michael S. Werner, Marc H. Claaßen, Tess Renahan, Mohannad Dardiry, and Ralf J. Sommer

Supplemental Information

Transparent Methods

Nematode strains and husbandry

P. pacificus Wild-type RS2333 (California) and RSC017 (La Réunion) strains were kept on 6 cm nematode growth media (NGM) plates seeded with OP50 and kept at 20°C. RSC017 is highly St and does not predate on other nematodes, and thus was used for biological assays instead of the highly Eu, predatory RS2333. To induce dauer, mixed-stage plates with little to no OP50 were washed with M9 and the resulting worm pellets were used in a modified 'White Trap' method. Worm pellets were placed on killed *Tenebrio molitor* grubs and dispersing dauers were collected in surrounding MilliQ water. Age of dauers ranged from one week to one month.

Dye staining

A stock solution of Neutral Red was prepared by dissolving 0.5 mg in 10 ml 5% acetic acid and stored at -20°C. Working solutions were prepared by 100x dilution in M9, aliquoted, stored at -20°C, and thawed directly before use. Working solutions were kept for approximately 1 month. Stock solutions of 10 mM CellTracker Green BODIPY were made in DMSO and stored at -20°C. J2s were prepared from 20-40 x 6 cm plates 6 days after passaging 5 worms to each plate on 300 µl OP50. Worms were washed from plates with M9 into a conical tube, and then filtered through 2 x 20 µM filters (Millipore) placed between rubber gaskets. The flow-through contained mostly J2 and some J3, which were pelleted by centrifugation, 8 seconds on a table-top eppendorf centrifuge 5424, reaching approximately 10,000 x g. The older/larger adult worms

remained on the filters, and were washed into a 50 ml conical tube with ~2 ml M9. Adults were then isolated by transferring worms to a 15 ml conical, and allowing them to swim/sink to the bottom of the tube. Adults reach the bottom faster than younger stages do, and after 3-5 rounds of removing supernatant and re-suspending in 2-3 ml M9, the pellet contains almost exclusively adults, which were re-suspended in 1 ml M9/50 µM Green BODIPY (Thermo Fisher). The J2 pellet was either directly re-suspended in 1 ml Neutral Red working solution, or in 1 ml M9 and split to two tubes, re-centrifuged, and re-suspended in 1 ml working solution Neutral Red (0.005% in M9) or 1 ml M9/50 µM Green BODIPY (Thermo Fisher). For the intermediate time point juveniles (J3s and some J4s), J2s isolated from 20 µM filtering were placed back on agar plates containing 300 µl OP50 bacterial food and grown for another 24 hours, and then washed from plates in M9 and re-filtered through 5 µM filters, then re-suspended in 1 ml 50 µM Green BODIPY (Thermo Fisher). Each tube was rotated for 3 hours in the dark at 20°C, then washed by centrifugation as before, and re-suspended in 1 ml M9. This was repeated 3-4x until the dye was no longer visible in the worm pellet. Then, the concentration of worms per microliter was determined by aliquoting 2 µl onto a glass coverslip in 5 technical replicates, and counted under a dissecting microscope. Finally the appropriate number of animals was added to 6 cm plates that had been previously seeded with 300 µl OP50, and incubated at 20°C. After 3 days, 100% of worms exhibited Neutral Red staining (*n*=50, Supplementary Figure 3). Dauers and J2s recovered after Neutral Red staining developed at the same developmental speed (3-4 days) and with the same mouth-form ratio as control worms recovered side-by-side (100% St for both, Supplementary Figure 4, *n*=30). Dauers and J2s stained with CellTracker Green BODIPY (50 µM) (Thermo) were similar, although less efficiently stained compared to Neutral Red. On day 4, 90% retained intestinal fluorescence (Supplementary Figure 3), and brightness decreased with the number of days. J2s in +/- 50 µM CellTracker Green BODIPY also developed at equivalent rates and mouth-form ratios (Supplementary Figure 4). Lower than 25 µM did not yield strongly

fluorescent worms after three hours. CellTracker Blue CMAC (Thermo Fisher) was also used at 50 µM and imaged 3 days post-staining for *P. pacificus*, and one day post-staining for *C. elegans*. However, due to the higher fluorescent background in the blue light spectrum in both *P. pacificus* and *C. elegans*, we performed all experiments using only Neutral Red and CellTracker Green BODIPY.

Microscopy

All images were taken on a Zeiss Axio Imager 2 with an Axiocam 506 mono, and processed using Zen2 pro software. Image brightness and contrast were enhanced in ImageJ with a minimum displayed value of 10 and maximum of 100 for all images in Figure 2, and Supplementary Figures 1 and 2, and a minimum of 21 and maximum of 117 for Supplementary Figure 3. The following exposure times were used for all images: Cy3 (peak emission = 561, exposure = 80 ms), FITC (peak emission = 519, exposure = 150 ms), Dapi (peak emission = 465, exposure = 80 ms), DIC (exposure = 80-140 ms).

Mixed culture experiments and statistical analysis

We performed the mixed culture experiments presented in Figure 3 with a minimum total number of counts $n > 100$, from three to five independent biological replicates for J2/24 hr, dauer, and adult competitor experiments, and two for the intermediate (J3/4) juvenile experiment (median counts per replicate for J2/24 hr=29, dauers=27, and adults=21, and avg. J3/4 counts was 75). J2 or dauers were stained with Neutral Red, then added to green-stained J2, dauer, J3/4, or adult populations as described in the 'Dye Staining' method section, on 6 cm plates with 300 µl OP50 and incubated at 20°C. To ensure consistent bacterial food supply, we added 1 ml more overnight OP50-LB to each plate on the following day, then air-dried under a chemical fume hood for 1 hour, then returned the plates to 20°C. On days three to four, we

phenotyped 'red' adults that exhibited no 'green' staining. To assess whether the age of the 'green' surrounding population affects the mouth form of the dependent variable 'red' J2s we performed a binomial regression on Eu counts (i.e. "successes") weighted by the number of counts per replicate, and the stage (juveniles vs. adults) and number added as a fixed effects, using a generalized linear model from the standard statistical package in R:

glm(formula=cbind(Eu,total)~'stage_added' * '#_added', data='J2/Da', family="binomial"))

See Supplementary Table S1 for a table containing the resulting *p* values. The AIC for our models (85.52 for juveniles and 72.32 for dauers) was substantially lower than the null hypothesis (220.16 for J2s and 147.29 for dauers), arguing a reasonable fit. For pair-wise comparisons of the effect of age for a given number of added animals, we performed a post-hoc Fisher's exact test on a contingency table containing the summed counts (n>100) of Eu and St observations against control plates (no added crowding animals). For display, we converted Eu counts into percent of total in Figure 3, with the *p* values for the number of animals added indicated over the relevant column (Significance codes: 0 '***' 0.001, '**' 0.01, '*' 0.05).

Measuring the effect of food depletion on mouth form

To verify that starvation was not a factor in our mixed culture experiments, we added increasing number of J2s to standard 6 cm plates with 300 µl OP50 to rapidly consume bacterial food, and measured both the amount of animals that reached adulthood, and the percent Eu in each population for two biological replicates. To assess the affects of added J2s to each dependent variable we performed a binomial regression with count data weighted by the total number of counts for each replicate:

glm(formula = cbind(reached_adult, total)~thousand_J2s, data=data_2, family="binomial"))

p values indicate a significant difference in percent reaching adult as a function of J2s added, but not in percent Eu (Table S1 bottom frame).

Supernatant collection and assays

Strains RS2333, RSC017, and RS2333-*daf-22.1;22.2* were raised in 10 ml liquid culture as in the time-resolved NDMM collections (see below). For each time point, 9 ml of the supernatant was lyophilized overnight, extracted again overnight with 90% ethanol (diluted in Millipore water) while being stirred, and centrifuged (4000 x g, 10 min, 4°C). The solvent was evaporated and the solid re-dissolved with 1 ml Millipore water. This clear extract was then directly used for the assays. One ml of the supernatant was cleaned for HPLC-MS analysis for quality control, as described in HPLC-MS sample preparation below. For the assays, RSC017 was synchronized by bleaching (Werner et al., 2017) and added to plates seeded with 300 µl OP50. The supernatants were added to the RSC017 J2s in two 500 µl increments (for a total of 1 ml supernatant) and dried for 30 minutes in a sterile hood after each addition. Plates were kept at 20°C and adult mouth forms were screened three days later. To determine significance a Fisher Exact test was performed on summed count data relative to S-medium control contingency tables, and the data are presented for representation as percentages in Figure 4.

HPLC-MS sample preparation for exo-metabolome and time resolved analysis

To collect staged pheromone profiles, we seeded 35 x 6 cm plates with 5 worms each, and bleached 5-6 days later when gravid to collect eggs/J1s. These were then added to 6 x 10 ml flasks with OP50 as described in Werner et al., 2017 (Werner et al., 2017). Then at 24, 48, or 72 hr time intervals, supernatants were obtained by centrifugation (>4,000 x g, 4°C for 10 minutes). 1 ml supernatant was adsorbed onto a SPE-C8 cartridge (Thermo Scientific Hypersep C8 100 mg/1ml), conditioned with 1 ml MeOH followed by 2 ml Millipore water. The adsorbed material was then washed with 200 µl water and subsequently eluted with 200 µl MeOH. This extract was then measured directly via HPLC-qTof MS (Bruker ImpactII).

125

126 **HPLC-MS measurement**

127 20 µl extract was injected into a Thermo UltiMate 3000 HPLC equipped with a Sigma-Aldrich
128 Ascentis Express C18 2.7 µm 10 mm x 4.6 mm column at 20°C with a flow of 500 µl/min. All MS
129 measurements have been performed in negative ion mode and molecules are detected as [M-
130 $H]^-$ Ions. The solvent gradient started with 5% acetonitrile (ACN)/ 95% water (both containing
131 0.1% formic acid) for 2 minutes. After this equilibration step, the ACN proportion was increased
132 to 65% over 8 min, then to 100% ACN in 1.2 minutes followed by a hold step for 8.8 minutes.
133 Afterwards, the system was flushed to 5% ACN with 2 minutes equilibration for a total of 22
134 minutes. For calibration, a sodium formate cluster building solution was automatically injected in
135 the first 2 minutes of each run. Data analysis was performed with TASQ version 1.0 from Bruker
136 Daltonics. Extracted ion chromatograms for each well-known compound with a mass width of
137 0.1 m/z and time slices of 0.5 minutes around the expected retention time were produced after
138 calibrating and baseline correction. Assignment errors were corrected with the provided MRSQ
139 value, and areas under the curve were calculated from the integral of each peak.

140

141 **Statistical analysis of NDMMs**

142 NDMM levels were compared simultaneously against strains and developmental stages by a
143 linear model in R: lm('NDMM' ~ 'developmental stage' * 'strain', data='data.frame')). In essence,
144 the linear model regressed the abundance of NDMMs against stage and strain as fixed effects.
145 *P* values between stages and strains were adjusted for multiple testing by a false discovery rate
146 correction (FDR). The level of fit between linear vs. exponential growth was determined by the
147 Akaike information criterion (AIC). The lowest AIC for iterations of different exponents
148 (n=1,2,3…) was used for comparison to the simple linear model. While significant in both cases,
149 for consistency we present the original *p* values from the original linear model in Table S2.

Supplemental Figure Legends

Figure S1, related to Figure 2. Vital dye staining of *Pristionchus pacificus*.

(A) Control *P. pacificus* imaged with Cy3, FITC, and DAPI filters, and a merge with Differential Interference Contrast (DIC). Histogram on the right represents quantification of intensity with each filter. (B) Same as (A) but stained with 0.005% Neutral Red, (C), 50 µM CellTracker Green BODIPY (Thermo Fisher), or (D) 50 µM CellTracker Blue CMAC Dye (Thermo Fisher). J2s were stained (see Transparent Methods), and ensuing adult animals were imaged 3 days later on a Zeiss Axio Imager 2 with an Axiocam 506 mono, and processed using Zen2 pro software. Image brightness and contrast were enhanced in ImageJ for display, with a minimum displayed value of 10 and maximum of 100 for all images. Note that while Neutral Red and CellTracker Green staining are bright and specific to their respective channels, CellTracker Blue is indistinguishable from background fluorescence.

Figure S2, related to Figure 2. Vital dye staining of *Caenorhabditis elegans.*

(A-D) Same as Supplementary Figure 1, but with *C. elegans*.

Figure S3, related to Figure 2. Vital dye staining of *P. pacificus* dauers, and duration of staining. (A) Control *P. pacificus* dauer imaged with DIC, Cy3, and FITC filters. (B) Dauers stained with either 0.005% Neutral Red or 50 µM CellTracker Green BODIPY and imaged immediately after staining with DIC, Cy3, and FITC filters and merged with DIC. Images were taken using Zeiss Axio Imager 2 with an Axiocam 506 mono, processed using Zen2pro software, and adjusted in ImageJ, with a display value minimum of 21 and maximum of 117.

(C-G) 50 µM CellTracker Green BODIPY and 0.005% Neutral Red-stained J2s were imaged every day for five days. Percent of individuals retaining the dyes are shown in panels next to each microscope image for each day. Both stains are seen in all organisms for three days; Neutral Red (NR) persists for at least five, while the number of Green BODIPY (GB) –stained worms drops on day four. All images are merged with DIC, n=31 GB, 63 NR day 1, 68 GB, 56 NR day 2, 50 GB, 50 NR day 3, 50 GB, 50 NR day 4, 50 GB, 50 NR day 5.

Figure S4, related to Figure 2. Vital dye staining does not affect *P. pacificus* mouth form or development.

(A) Neutral Red and CellTracker Green BODIPY-stained J2s reach adulthood at the same rate as unstained J2s (3 days). (B) All of the J2s stained retain the dye in adulthood in the intestine. (C) Neither dye affects mouth form; both unstained and stained worms remain 100% St (n=30). (D-F) Same as for (A-C) except with dauers instead of J2s, and only with Neutral Red. (G) Developmental rate of J2 unstained, Neutral Red-stained (NR), and CellTracker Green BODIPY-stained (GB) RSC017 every 12 hours post-J2 staining. Two biological replicates, n=60. To see if there were significant differences between stained and un-stained, a Fisher's Exact test was performed on summed counts of each stage (all $p>0.05$) (H) Staging of RSC017 worms from liquid culture at the relevant time points, 24 hrs, 48 hrs, and 72 hrs. Error bars represent standard error of the mean for 3 biological replicates, n>100 animals counted per replicate.

Table S1, related to Figure 3. Table of binomial regression *p* values for crowding assays.

Significance *p* values from binomial regression of vital-dye method for age and number added, and from binomial regression of number-reaching-adult and Eu counts, for each number of individuals added relative to 1,000 individuals added (see Transparent Methods for details).

Figure S5, related to Figure 5. Pheromone profiling quality control.

(A) Extracted ion traces (width 0.1 m/z) of 11 of the 12 NDMMs used in this publication from a seven-day mixed-stage sample, double peak of 247.12 m/z indicate isomeric structures (Part#9/Ascr#9). (B) Example of an averaged spectrum over a calibration segment; sodium-formate cluster building solution was used to ensure high mass accuracy in each run. (C) Comparison of an endometabolome sample from a seven- day mixed-stage cultured compared to the endometabolome of eggs, produced by using bleached eggs from 80 x 60 mm plates.

Table S2, related to Figure 5. Table of linear regression *p* values with FDR corrections for strain and stage comparison of NDMM levels. FDR-corrected and uncorrected *p* values from linear regression of *P. pacificus* NDMMs (alternating grey background between NDMMs for clarity). Red values indicate FDR<0.05.

Table S3, related to Figure 5. P values from pairwise comparison of dasc#1, npar#1, and ascr#9 throughout development. Significance assessed with a two-tailed student's *t*-test. Top table indicates comparison of raw pheromone levels experienced by worms, and the bottom table indicates comparison of volume-normalized pheromone levels (normalized data from WormSizer (Moore et al., 2013), Fig. S6B-D).

Figure S6, related to Figure 5. Enzyme that synthesizes NDMMs is transcriptionally regulated during development, and volume normalization of pheromones. (A) Comparison of *daf-22.1* (FPKM) by RNA-seq through different stages of development, data from Baskaran et al., 2015 (Baskaran et al., 2015). A two-sided students *t*-test was performed between 56-68

hours (J4-adults) and 22 hours (J2s) (Significance codes: 0 '***' 0.001, '**' 0.01, '*' 0.05). (B) Representative images of worms raised in liquid culture at 24 hrs, 48 hrs, and 72 hrs. (C) Comparison of worm volumes (picoLiters) for 24 hrs, 48hrs, and 72 hrs, using WormSizer (Moore et al., 2013). (D) Time-resolved NDMM levels of RSC017 normalized by worm volume (upper graph) and unnormalized (lower graph, also shown in Figure 5B). Data is presented as the mean of nine biological replicates and error bars represent standard error of the mean (SEM). In the upper graph, levels were normalized to worm volume based on the data shown in (C).

Table S4, related to Figure 5. Raw and volume-normalized data of RSC017 pheromones, in absolute value of area under the curve. Normalization of 48 hr and 72 hr time point abundances relative to 24 hrs. Average volumes obtained by WormSizer (Moore et al., 2013)(Figure S6B-C).

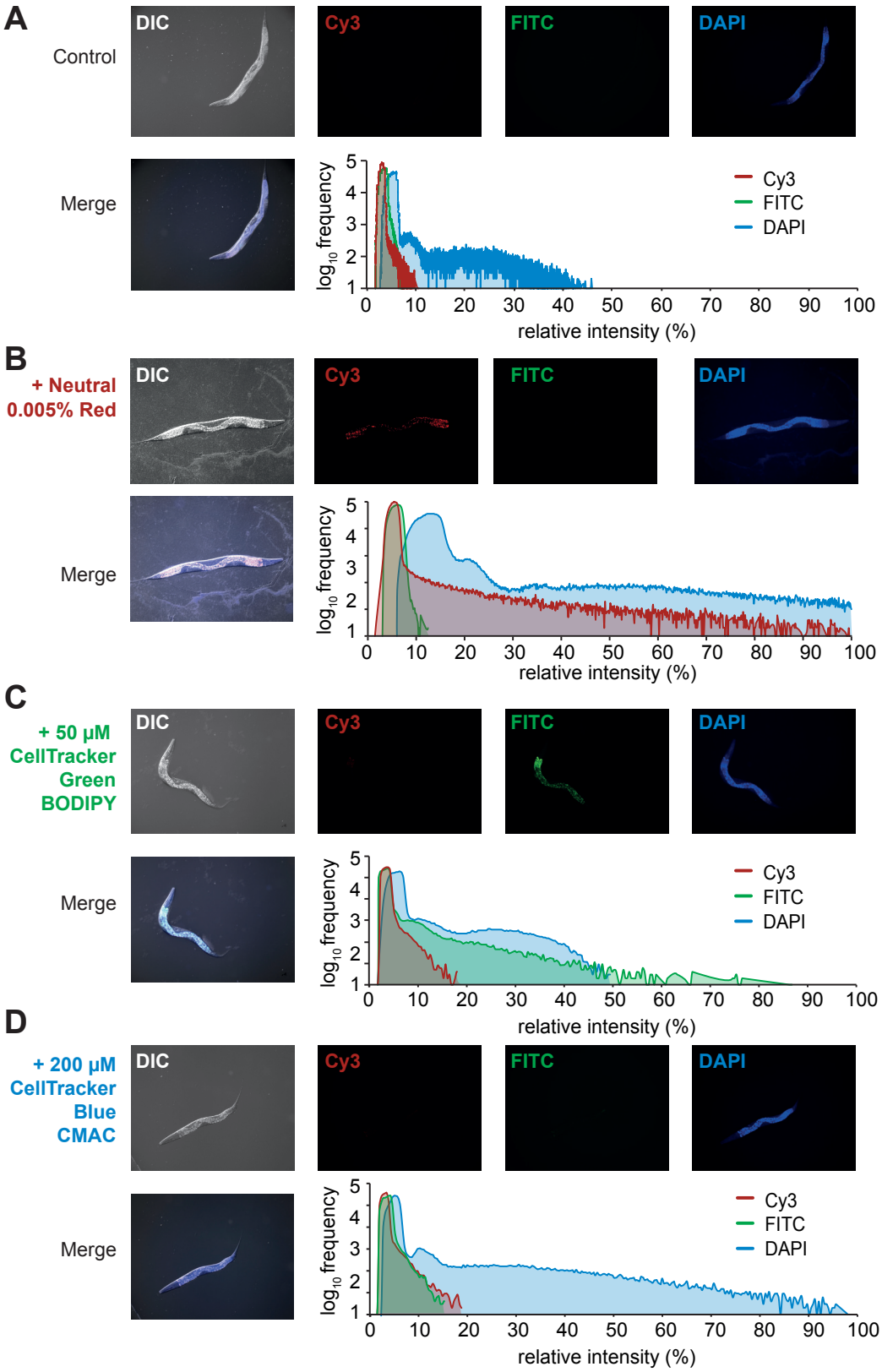

Figure S1, related to Figure 2. Vital dye staining of *Pristionchus pacificus*.

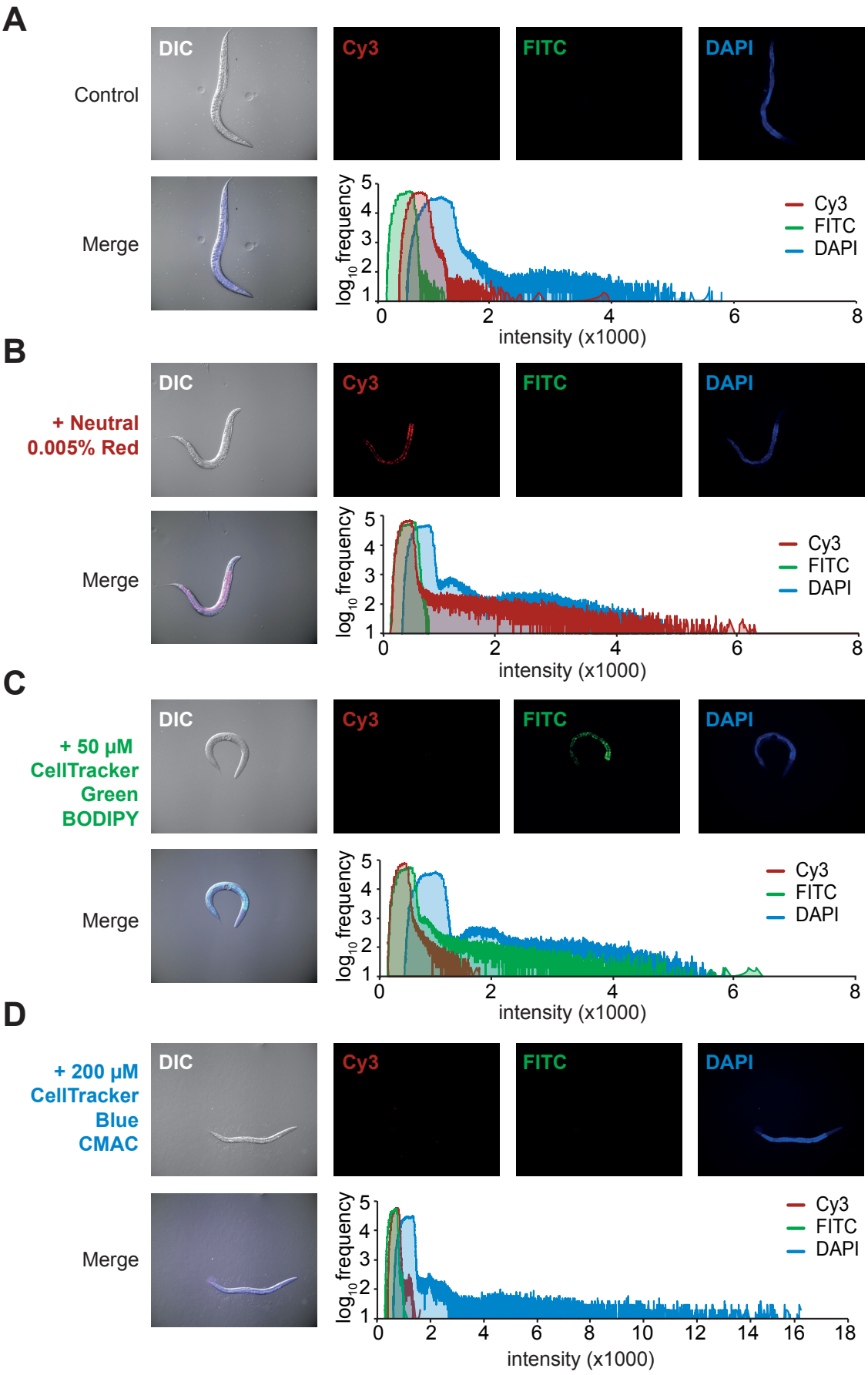

Figure S2, related to Figure 2. Vital dye staining of *Caenorhabditis elegans*.

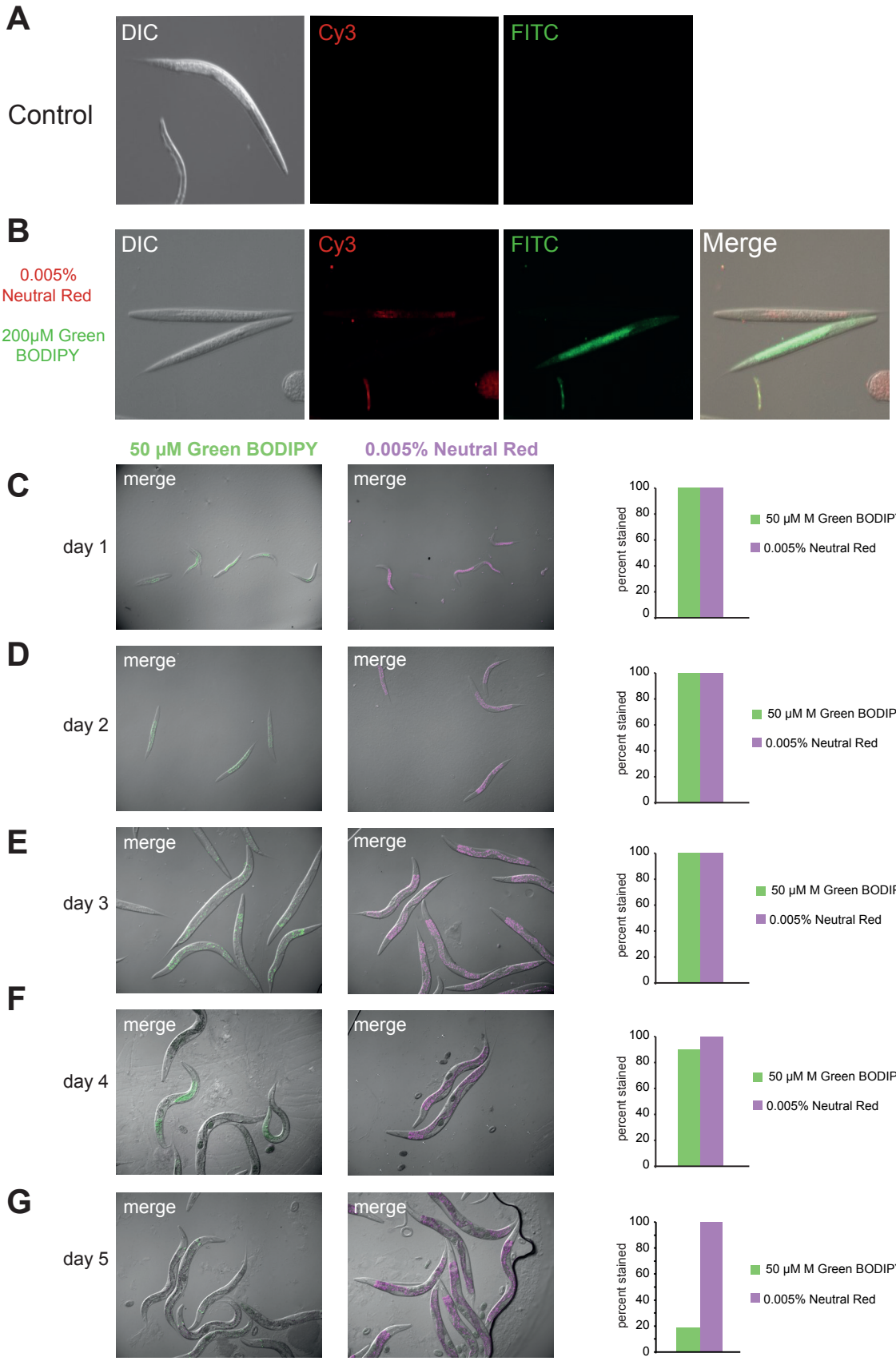

Figure S3, related to Figure 2. Vital dye staining of *Pristionchus pacificus* dauers, and duration of staining.

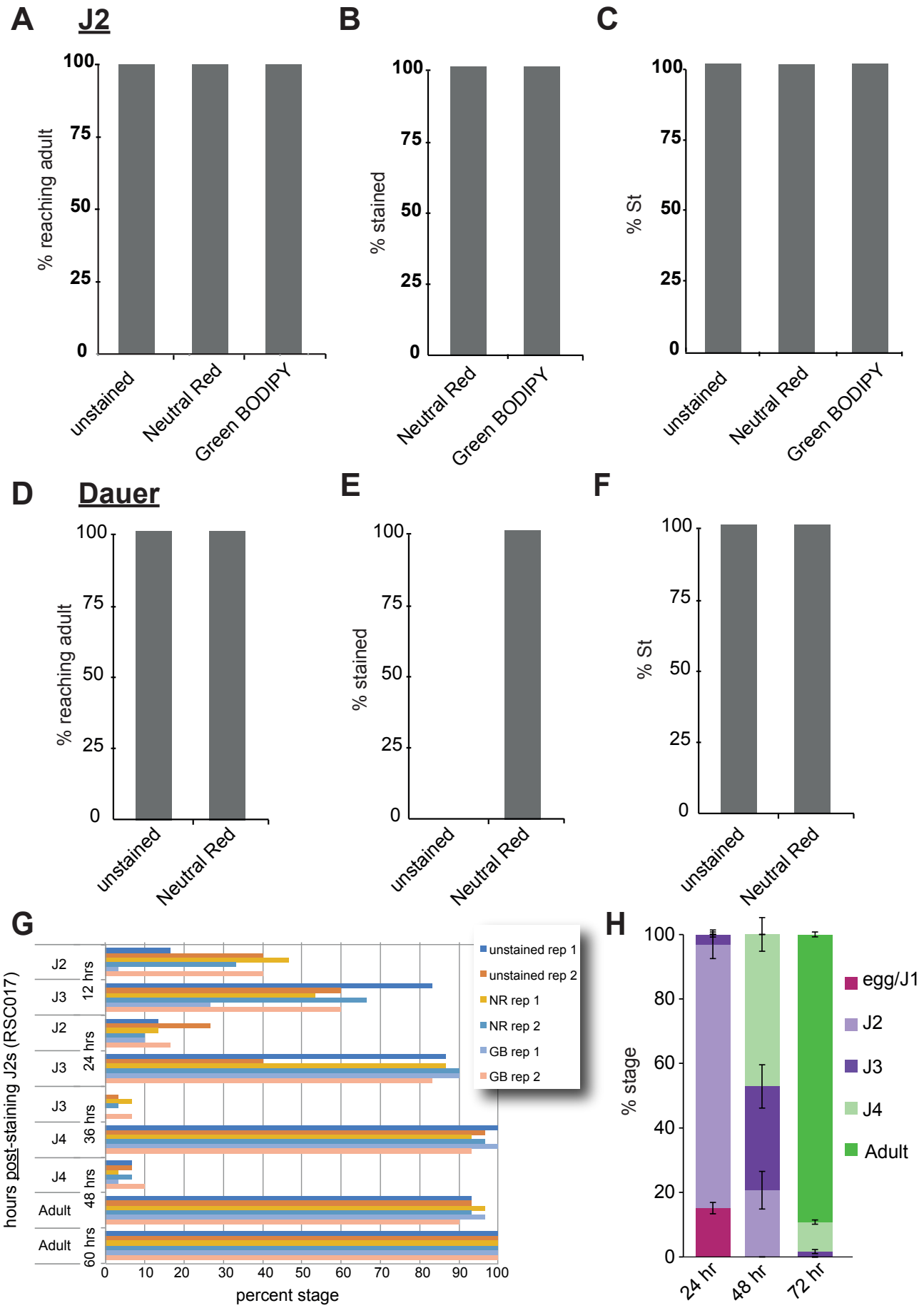

Figure S4, related to Figure 2. Vital dye staining does not affect P. pacificus mouth form or development.

effect of population age on mouth form of developing juveniles

binomial regression	*p* value red-stained J2s	*p* value red-stain dauers
stage added (adults vs. juveniles)	0.0132	0.002955
number added	4.28e-13	0.000404

effect of number of peers on development and mouth form (proxy for potential starvation effects on mouth form)

binomial regression	*p* value for development (relative to 1,000)	*p* value for Eu (relative to 1,000)
3,000 J2s added	0.3408	1.0
4,000 J2s added	0.0424	1.0
5,000 J2s added	6.06E-14	0.99
10,000 J2s added	4.09E-14	0.99

Table S1, related to Figure 3. Table of binomial regression p values for vital-dye method and excess crowding.

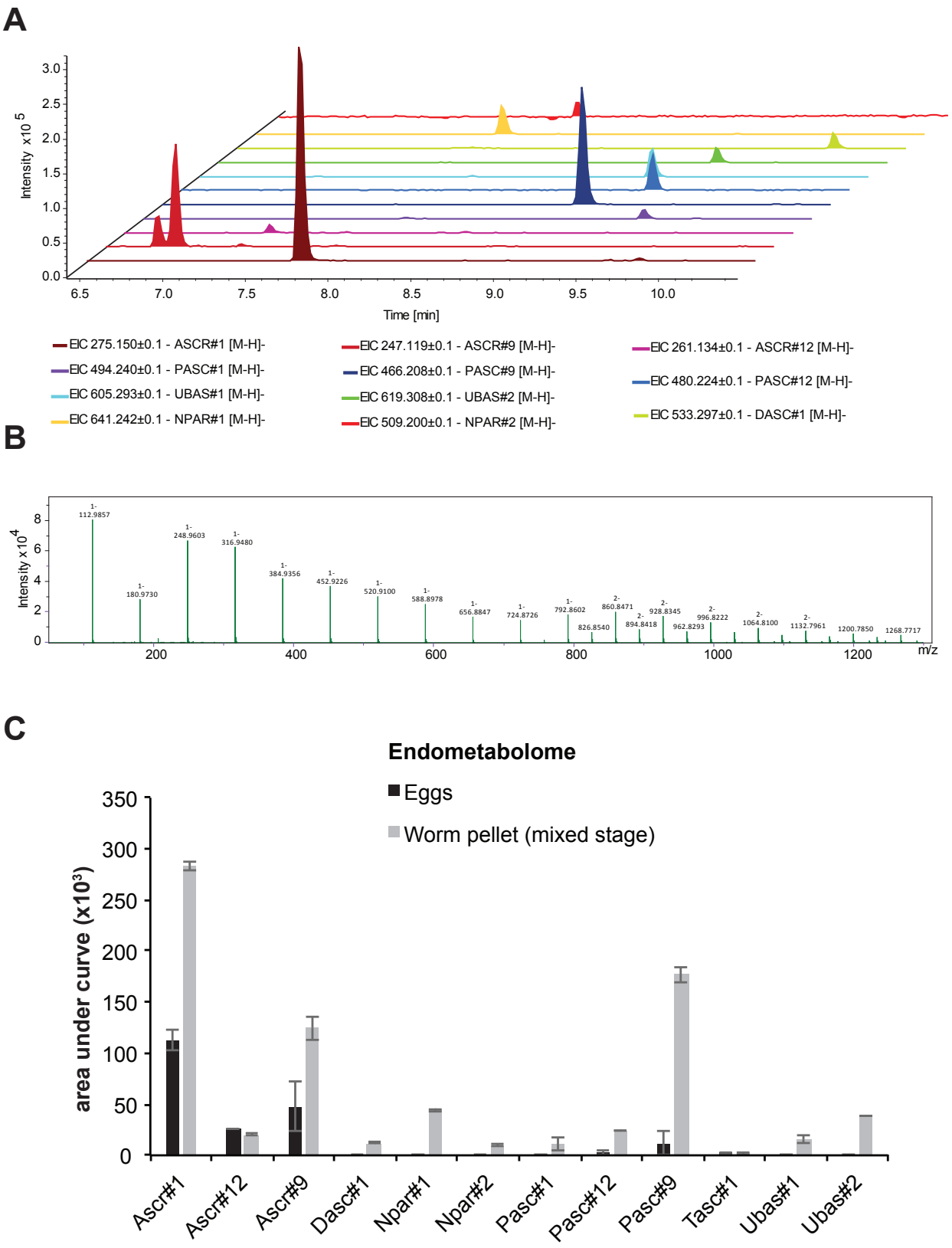

Figure S5, related to Figure 5. Pheromone profiling quality control

NDMM comparison	pvalue	fdr corrected
ascr1_stage	0.4733	0.774490909
ascr1_strain	0.0429	0.110314286
ascr1_stage:strain	0.031	0.085846154
ascr9_stage	3.79E-05	0.0002274
ascr9_strain	0.651	0.778064516
ascr9_stage:strain	0.272	0.50148
ascr12_stage	0.0029	0.01404
ascr12_strain	0.0897	0.201825
ascr12_stage:strain	0.0302	0.085846154
dasc1_stage	9.62E-08	8.66E-07
dasc1_strain	0.11363	0.240628235
dasc1_stage:strain	0.00351	0.01404
npar1_stage	0.0033	0.01404
npar1_strain	0.9426	0.984
npar1_stage:strain	0.6355	0.778064516
npar2_stage	0.0516	0.12384
npar_2strain	0.984	0.984
npar2_stage:strain	0.9716	0.984
pasc1_stage	0.449	0.769714286
pasc1_strain	0.753	0.847125
pasc1_stage:strain	0.564	0.778064516
pasc9_stage	0.616	0.778064516
pasc9_strain	0.267	0.50148
pasc9_stage:strain	0.523	0.778064516
pasc12_stage	0.6122	0.778064516
pasc12_strain	0.2786	0.50148
pasc12_stage:strain	0.67	0.778064516
tasc1_stage	0.522	0.778064516
tasc1_strain	0.862	0.940363636
tasc1_stage:strain	0.57	0.778064516
ubas1_stage	3.13E-12	1.13E-10
ubas1_strain	0.00538	0.019368
ubas1_stage:strain	6.69E-08	8.03E-07
ubas2_stage	1.34E-11	2.41E-10
ubas2_strain	0.00711	0.023269091
ubas2_stage:strain	6.18E-07	4.45E-06

Table S2, related to Figure 5. Table of linear regression *p* values with *FDR* correction for strain and stage comparison of NDMM levels.

RS2333	dasc#1	npar#1	ascr#9
72 hrs compared to 24 hrs	5.75E-07	3.47E-05	1.03E-04
72 hrs compared to 48 hrs	5.71E-03	1.76E-01	1.97E-01
RSC017	dasc#1	npar#1	ascr#9
72 hrs compared to 24 hrs	2.55E-02	3.66E-03	2.03E-02
72 hrs compared to 48 hrs	2.12E-01	3.66E-01	1.04E-01

Volume normalized

RS2333	dasc#1	npar#1	ascr#9
72 hrs compared to 24 hrs	5.75E-07	3.47E-05	1.02E-03
72 hrs compared to 48 hrs	1.44E-02	2.92E-01	6.21E-01
RSC017	dasc#1	npar#1	ascr#9
72 hrs compared to 24 hrs	2.55E-02	3.66E-03	4.34E-02
72 hrs compared to 48 hrs	2.71E-01	5.46E-01	1.70E-01

Table S3, related to Figure 5. P values from pairwise comparison of dasc#1, npar#1, and ascr#9 throughout development.

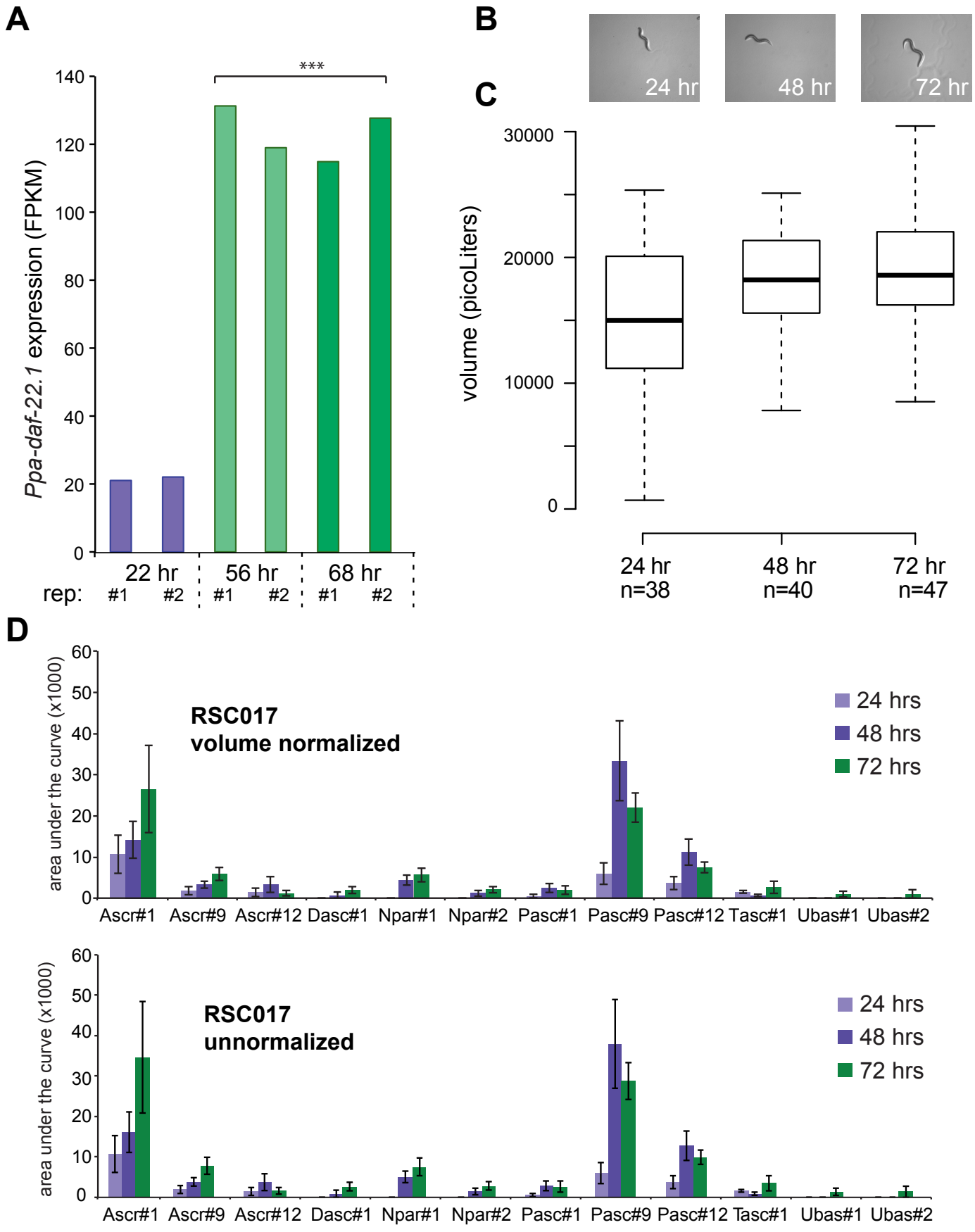

Figure S6, related to Figure 5. Enzyme that synthesize NDMMs is transcriptionally regulated during development, and volume normalization of pheromones.

STAGE	DASC1	NPAR1	Pasc9	Ascr1	Ascr12	Ascr9	Npar2	Pasc1	Pasc12	Tasc1	Ubas1	Ubas2
24	0	0	0	0	0	0	0	0	0	1610	0	0
24	0	0	0	4489	0	0	0	0	0	1214	0	0
24	0	0	0	0	0	0	0	0	0	1769	0	0
24	0	0	0	22265	0	4301	0	0	0	1169.5	0	0
24	0	0	0	28319.5	0	5450	0	0	0	1871.5	0	0
24	0	0	7193.5	35197.5	8299.5	7177	0	0	9476	3918	0	0
24	0	0	16048.5	3929.5	5028.5	0	0	0	8318	969.5	0	0
24	0	0	19293.5	2386.5	0	0	0	1657.5	11094	999	0	0
24	0	0	11623.5	0	0	0	0	3667.5	4799.5	949.5	0	0
48	7800	8901	111298	7866	0	4250	6050	8486	35583.5	2827	0	0
48	0	8393	54479	7660	0	7077	5605	6699	19222.5	1047.5	0	0
48	0	10347	32381.5	11133	0	4339	0	6513	11901.5	2324	0	0
48	0	0	13819	34084	16659.5	5087	0	0	5916	1217	0	0
48	0	0	6893	40108	12167	7298	0	0	0	0	0	0
48	0	0	6766	32972	5415	6235.5	0	0	0	0	0	0
48	0	7635.5	56471.5	6725	0	0	1522	3957	17663.5	400.5	0	0
48	0	7036	29685.5	4781	0	0	0	0	13964.5	0	0	0
48	0	3205.5	29656	0	0	0	0	0	10977	0	0	0
72	0	16111.5	45664.5	9007	0	7593.5	5065	10394.5	17614.5	2243	0	12581
72	6321	9157.5	36161.5	7275	0	5649	5062	8322	13492	562.5	0	0
72	4475.5	17381	51388	7354.5	0	7472	7192	5269.5	12932	1192	0	0
72	7400.5	10075	25671	93903	6060	22877	6485	0	8342	12416	6377.5	0
72	0	0	9248.5	61584	3670.5	7879	0	0	0	14621	0	0
72	5861	0	13904	107297	4907.5	8875	0	0	5734	0	5697.5	0
72	0	0	20159.5	12767.5	0	0	0	0	9426	0	0	0
72	0	7294.5	28800	6249	0	3823	0	0	7802	544	0	0
72	0	7454.5	28094	6695.5	0	6082	1696.5	0	13884.5	201	0	0

RSC017 pheromone levels

STAGE	DASC1	NPAR1	Pasc9	Ascr1	Ascr12	Ascr9	Npar2	Pasc1	Pasc12	Tasc1	Ubas1	Ubas2
24	0	0	0	0	0	0	0	0	0	1610	0	0
24	0	0	0	4489	0	0	0	0	0	1214	0	0
24	0	0	0	0	0	0	0	0	0	1769	0	0
24	0	0	0	22265	0	4301	0	0	0	1169.5	0	0
24	0	0	0	28319.5	0	5450	0	0	0	1871.5	0	0
24	0	0	7193.5	35197.5	8299.5	7177	0	0	9476	3918	0	0
24	0	0	16048.5	3929.5	5028.5	0	0	0	8318	969.5	0	0
24	0	0	19293.5	2386.5	0	0	0	1657.5	11094	999	0	0
24	0	0	11623.5	0	0	0	0	3667.5	4799.5	949.5	0	0
48	6859.790284	7828.076066	97882.17167	6917.834663	0	3737.706244	5320.734771	7463.100045	31294.27533	2486.234248	0	0
48	0	7381.310238	47912.11729	6736.665843	0	6223.940492	4929.374941	5891.504502	16905.42548	921.2346567	0	0
48	0	9099.77565	28478.24347	9791.03144	0	3815.97821	0	5727.924887	10466.89667	2043.86572	0	0
48	0	0	12153.26179	29975.52462	14651.36875	4473.81451	0	0	5202.887092	1070.303176	0	0
48	0	0	6062.119798	35273.39342	10700.39338	6418.301217	0	0	0	0	0	0
48	0	0	5950.428341	28997.56477	4762.277486	5483.874656	0	0	0	0	0	0
48	0	6715.119066	49664.44193	5914.370469	0	0	1338.538566	3480.024379	15534.34688	352.2238473	0	0
48	0	6187.88262	26107.21852	4204.69966	0	0	0	0	12281.22326	0	0	0
48	0	2819.109969	26081.27444	0	0	0	0	0	9653.835634	0	0	0
72	0	12340.85154	34977.427	6899.050356	0	5816.358263	3879.61475	7961.827348	13492.09753	1718.060392	0	9636.610695
72	4841.667292	7014.328149	27698.45781	5572.398284	0	4326.938544	3877.316854	6374.364057	10334.40517	430.8555374	0	0
72	3428.078147	13313.24461	39361.42997	5633.292533	0	5723.293467	5508.823155	4036.254674	9905.46455	913.0307566	0	0
72	5668.526941	7717.101403	19663.09778	71926.44894	4641.750323	17522.99045	4967.285618	0	6389.683365	9510.226404	4884.944337	0
72	0	0	7084.031	47171.21318	2811.476	6035.041385	0	0	0	11199.18011	0	0
72	4489.323208	0	10649.98292	82185.7895	3758.9752	6797.942923	0	0	4392.045603	0	4364.087865	0
72	0	0	15441.47948	9779.463242	0	0	0	0	7219.989859	0	0	0
72	0	5587.334609	22059.80351	4786.517783	0	2928.285723	0	0	5976.062049	416.6851775	0	0
72	0	5709.889073	21519.03194	5128.521334	0	4658.601562	1299.460301	0	10635.04659	153.9590454	0	0

RSC017 volume normalized pheromone levels

Table S4, related to Figure 5. Raw and normalized data of RSC017 pheromones, in absolute value of area under the curve.